

UNCLASSIFIED

AD 409 015

DEFENSE DOCUMENTATION CENTER

FOR

SCIENTIFIC AND TECHNICAL INFORMATION

CAMERON STATION, ALEXANDRIA, VIRGINIA



UNCLASSIFIED

NOTICE: When government or other drawings, specifications or other data are used for any purpose other than in connection with a definitely related government procurement operation, the U. S. Government thereby incurs no responsibility, nor any obligation whatsoever; and the fact that the Government may have formulated, furnished, or in any way supplied the said drawings, specifications, or other data is not to be regarded by implication or otherwise as in any manner licensing the holder or any other person or corporation, or conveying any rights or permission to manufacture, use or sell any patented invention that may in any way be related thereto.

N-63-4-2

409 015

CATALOGED BY DDC

AS AD NO. 409015

DEVELOPMENT OF BARIUM OXIDE - URANIUM OXIDE - TUNGSTEN  
AND BARIUM OXIDE - URANIUM OXIDE - RHENIUM EMITTERS  
FOR USE IN NUCLEAR HEATED THERMIONIC CONVERTERS

ANNUAL REPORT

FOR

Nonr-3870(00)

July 1, 1963

General Motors Research Laboratories  
Warren, Michigan

DEVELOPMENT OF BARIUM OXIDE-URANIUM OXIDE-TUNGSTEN  
AND BARIUM OXIDE-URANIUM OXIDE-RHENIUM EMITTERS  
FOR USE IN NUCLEAR HEATED THERMIONIC CONVERTERS

ANNUAL REPORT  
FOR  
NONR-3870(00)

JULY 1, 1963

GENERAL MOTORS RESEARCH LABORATORIES  
WARREN, MICHIGAN

This report has been prepared under Contract  
No. Nonr-3870(00) for the Office of Naval Research.  
The contract was funded by the Bureau of Ships. It  
was technically supervised through the Office of  
Naval Research by Dr. J. J. Connelly, Jr., Commander  
U. S. Navy and Mr. B. Rosenbaum.

(a)

Office of Naval Research  
Contract Nonr-3870(00)

DEVELOPMENT OF BARIUM OXIDE-URANIUM OXIDE-TUNGSTEN  
AND BARIUM OXIDE-URANIUM OXIDE-RHENIUM EMITTERS  
FOR USE IN NUCLEAR HEATED THERMIONIC CONVERTERS

Authors

Fay E. Gifford  
Robert F. Hill

Report for Period June 1, 1962 to June 30, 1963

General Motors Research Laboratories  
Warren, Michigan

Reproduction in whole or in part is permitted  
for any purpose of the United States Government

FOREWORD

This report for the period June 1, 1962 to June 30, 1963 covers the research program related to the development and testing of various barium-uranium emitter materials. The following sections on Abstract, Conclusions and Future Plans gives the substance of the main body of the report in condensed form.

The work in this contract was directed toward the fabrication, operation and testing of unclad nuclear thermionic emitters that could be operated in the 1100-1300°C temperature range with an expected current density of 1 - 10 amp/cm<sup>2</sup>. Various nuclear fuels impregnated with an activating agent were to be evaluated both from the standpoint of physical and chemical properties as well as electron emission characteristics. The most promising nuclear fuel emitter materials were to be selected and evaluated on the basis of x-ray analysis, evaporation rate and electron emission.

ABSTRACT

Thermionic energy converters, which presently use unclad nuclear fuel emitters, operate in a high temperature region (1700-2000°C) due to the electron emission characteristics of the emitter. In this temperature region, the life of the emitter is much lower than desired due to evaporation of the emitter material. A possible solution to this problem is to operate the nuclear heated thermionic emitter at a much lower temperature (1100-1300°C) where evaporation of the nuclear fuel in the emitter would be negligible over long periods of time. This report is concerned with the research and development of nuclear heated emitters that can be operated in the 1100 to 1300°C range with an electron emission capability of 1 to 10 amps/cm<sup>2</sup>.

The results of this program are summarized in three major sections:

- A. Material Studies
- B. Emission Studies
- C. Emission Microscope Studies



#### A. Material Studies

The materials program was concerned with the development of various barium-uranium emitter materials. Emitter materials containing BaO,  $\text{UO}_2$ , UC, W and Re were evaluated. Preliminary compatibility studies indicated that the barium oxide-uranium carbide system was not chemically stable, while the barium oxide-uranium oxide system appeared very promising. Materials containing various concentrations of BaO in  $\text{UO}_2$  were fabricated into dense compacts and evaluated on the basis of x-ray analysis, evaporation rate and chemical thermodynamics. The metallurgical examinations indicated that barium oxide and uranium dioxide form several compounds of which  $\text{BaUO}_3$  and  $\text{Ba}_2\text{UO}_4$  were identified. The evaporation rate studies and the thermodynamic calculations indicated that the BaO- $\text{UO}_2$ -W emitter materials were comparable to the BaO- $\text{Al}_2\text{O}_3$ -W emitter materials that are presently being employed in the Philips impregnated cathode emitters.

#### B. Emission Studies

Electron emission studies were made on sixteen different compositions of barium-uranium emitters. The results indicated that electron current densities in the vicinity of 10 amps/cm<sup>2</sup> can be obtained from the BaO- $\text{UO}_2$ -W and the BaO- $\text{UO}_2$ -Re emitter systems. The high current densities were obtained in the 1200°C region where the barium evaporation rate was measured to be  $1 \times 10^{-5}$  gm/cm<sup>2</sup>-hr. In general, the higher the barium content the higher was the emission current for a given temperature. The emission characteristics of the various emitter materials were very reproducible after they had been properly activated.

In order to aid in the evaluation of the large quantity of emission data, a code for use on the IBM-7090 was established. The correlations were achieved by obtaining a least square fit of the data to the Schottky and Richardson equations. Emission constant, work function and work function temperature coefficient were calculated for the various input data.

#### C. Emission Microscope Studies

Experiments were conducted on the thermionic emission microscope in order to evaluate its usefulness for studying the emission characteristics of the various emitter materials. The results of the experiments indicated that the emission microscope can be used to obtain qualitative information on the surface structure of emitters--such as the degree of barium coverage, but quantitative information such as work function and emission constant cannot be obtained readily.

### Conclusions

The results from the material and electron emission studies that have been conducted on the various BaO-UO<sub>2</sub>-W and BaO-UO<sub>2</sub>-Re emitter materials indicate that these materials are comparable to the BaO-Al<sub>2</sub>O<sub>3</sub>-W emitter materials that are presently employed in the Philips cathode emitters. In order to obtain a balance between the emission properties as determined by the barium oxide content and the nuclear characteristics as determined by the uranium dioxide content, emitters containing 60 mole percent barium oxide and 40 mole percent uranium dioxide were selected for detail future testing. Emitters containing 75 volume percent of this oxide mixture and 25 volume percent tungsten had a work function of 2.21 ev and an electron emission current capability of 8.9 amps/cm<sup>2</sup> at 1200°C. At this temperature the evaporation rate of this material was approximately  $9 \times 10^{-6}$  gm/cm<sup>2</sup>-hr. Based on this information the emitter material containing 60 m/o BaO and 40 m/o UO<sub>2</sub> appeared the most promising.

### FUTURE PLANS

In order to evaluate the characteristics of the 60 m/o BaO - 40 m/o UO<sub>2</sub> system in a nuclear environment, various emitter specimens containing enriched uranium (U-235) will be fabricated and tested in the University of Michigan reactor. Since the oxide particle size had very little influence on the physical and emission properties of the fabricated emitters, oxide particles of minus 100 mesh and tungsten powder of minus 300 mesh will be used throughout. Samples containing 25, 50 and 75 v/o tungsten, the remainder being the oxide mixture, will be fabricated and tested. The various tests will involve:

- 1) non-nuclear electron emission studies in the laboratory using electrical heat only,
- 2) electron emission studies in a nuclear reactor environment,
- 3) transportation studies (evaporation under thermionic emission conditions),
- and 4) electron microprobe analysis of the emitter surface.

Development of Barium Oxide - Uranium Oxide - Tungsten  
and Barium Oxide - Uranium Oxide - Rhenium Emitters  
for use in Nuclear Heated Thermionic Converters

CONTENTS

	<u>Page</u>
I. INTRODUCTION	1
II. MATERIAL STUDIES	1
A. PERLIMINARY COMPATIBILITY STUDIES	2
B. BaO-UO <sub>2</sub> SYSTEM	4
C. BaO-UO <sub>2</sub> EMITTER MATERIAL STUDIES	6
1. X-Ray Analysis	7
2. Microstructure Analysis	8
3. Evaporation Rate Data	10
4. Density Determination	15
5. Thermodynamics of the Barium Oxide-Uranium Oxide System	16
D. EMITTER SAMPLES	20
III. EMISSION STUDIES	22
A. APPARATUS	22
1. Vacuum System	22
a. Pumps	24
b. Liquid Nitrogen Trap	24
c. Vacuum Manifold	25
d. Portable Bakeout Oven and Power Supply	27
2. Tubes	29
a. Emitter - Collector Arrangement	30
b. Tube Base and Gasket Seal	31
c. Heaters	32
3. High Voltage Pulser	32
B. OPERATING PROCEDURE	35
1. Tube Processing	35
2. Emitter Processing	35
3. Emitter Temperature Calibration	36

CONTENTS (Continued)

	<u>Page</u>
C. THERMIONIC EMISSION	38
1. Basic Equations	38
2. Experimental Data	40
3. Data Evaluation	41
IV. EMISSION MICROSCOPE STUDIES	53
A. BARIUM OXIDE - URANIUM OXIDE EMITTERS	53
B. PHILIPS CATHODE EMITTER	54
C. EMISSION CURRENT	58
V. REFERENCES	64
VI. ACKNOWLEDGMENTS	65
VII. DISTRIBUTION	66

## I. INTRODUCTION

The major development of emitter materials for use in nuclear heated thermionic diode converters has been limited almost exclusively to compounds that contain uranium carbide. These systems will supply adequate electron emission currents only when heated to temperatures in the vicinity of  $1700^{\circ}\text{C}$ .<sup>(1)</sup> The problems encountered with most emitter materials at these high temperatures have been concerned with their mechanical and chemical stability. The evaporation rate of the emitter material is one of the major problems. In order to reduce the high temperature requirements, a materials program was initiated with the aim of developing an emitter that would contain uranium and that could be operated in the temperature range of  $1100$  to  $1300^{\circ}\text{C}$  with an electron emission capability of  $1\text{--}10$  amps/cm<sup>2</sup>.

In the past ten years the practical utilization of impregnated emitters has commanded a great deal of interest, especially in cases where it is necessary to obtain comparatively large electron emission current densities at moderate temperatures. Such emitters generally consist of a porous matrix containing an appropriate activating agent, usually barium oxide. Under actual operating conditions, the barium oxide is reduced to free barium atoms. These free barium atoms then diffuse through the porous matrix onto the external surface, where they cover the emitting surface producing the desired emission characteristics. On this basis it appeared feasible to develop a nuclear heated emitter that would embody a fissile fuel such as UC or  $\text{UO}_2$  and an activating agent such as barium oxide.

## II. MATERIAL STUDIES

The development of barium-uranium emitters involved two specific problems. The first and foremost problem was the chemical compatibility of the various constituents of the emitter. In the Philips dispenser-type emitter, fused tribarium aluminate is impregnated into a tungsten matrix. During activation and operation, the tribarium aluminate is decomposed to barium oxide and monobarium aluminate, in which case the latter compound is chemically inert with the tungsten. The barium oxide, on the other hand, is further reduced to free barium atoms by the tungsten. The production rate of the free barium atoms is regulated by controlling the activity of the BaO through the use of  $\text{BaO-Al}_2\text{O}_3$  mixtures (namely tribarium aluminate) and by controlling the activity of the tungsten by alloying it with molybdenum. In the barium-uranium emitters the complexity of the chemical reactions may greatly be increased by the introduction of the fissile fuel. For example, reactions between the barium oxide and the

uranium carbide may be so extensive that a very short emitter life will exist. On the other hand, the formation of complex barium oxide-uranium oxide compounds may reduce the activity of the barium oxide to such a low level that reasonable electron emission currents cannot be obtained from the emitter.

The other problem involved the actual fabrication of the emitters. Problems involving blending and compacting of the various powders had to be investigated from the standpoint of density, homogeneity and bonding. In order to gain an insight into the chemical stability of various barium oxide-uranium compound mixtures, some preliminary compatibility studies were conducted. The results of these studies are presented below.

#### A. PRELIMINARY COMPATIBILITY STUDIES

Cursory investigations of the chemical stability of several potential combinations of emitter materials were conducted. The initial compatibility tests were limited to tribarium aluminate and various uranium compounds. The tribarium aluminate was prepared by blending 85 w/o  $\text{BaCO}_3$  powder with 15 w/o  $\text{Al}_2\text{O}_3$  powder. After blending, the mixture was poured into a mullite tube and heated in air to approximately  $1800^\circ\text{C}$  where the material became molten. After cooling, the material was transferred to an argon filled dry box where it was crushed to a powder. X-ray analysis of the powder revealed a pattern of  $\text{BaAl}_2\text{O}_4$  instead of the intended  $\text{Ba}_3\text{Al}_2\text{O}_6$ . Metallographic examination of this material, however, revealed a two-phase structure. Either an alumina pickup during melting of the material in the mullite crucible or a barium oxide loss by vaporization was sufficient to result in a composition between  $\text{BaAl}_2\text{O}_4$  and  $\text{Ba}_3\text{Al}_2\text{O}_6$ ; with  $\text{BaAl}_2\text{O}_4$  being the predominate phase. This material was used in the subsequent experiments and was referred to as  $\text{BaAl}_2\text{O}_4$ .

The resulting barium aluminate powder was then combined with either UC or  $\text{UO}_2$  powder to form compacts with compositions of 75 w/o UC - 25 w/o  $\text{BaAl}_2\text{O}_4$  and 60 w/o  $\text{UO}_2$  - 40 w/o  $\text{BaAl}_2\text{O}_4$ . These compositions resulted in approximately equal specific volume loadings of uranium compounds. These compacts along with compacts of  $\text{BaAl}_2\text{O}_4$ , UC and  $\text{UO}_2$  were then loaded into tantalum tubes for densification. The powder compacts, arranged in the tantalum tubes as shown in Fig. 1, were densified by gas-pressure bonding for 3 hours at  $1500^\circ\text{C}$  under a helium gas pressure of 10,000 psi.

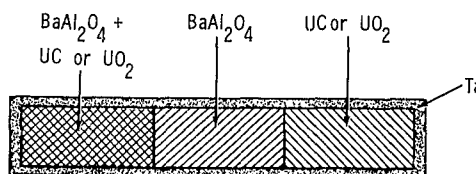


Figure 1 - Arrangement of compacts in tantalum tube.

After densification, the tantalum cladding was removed and the samples were examined metallographically. The interfaces between the barium aluminate and the uranium compounds were investigated for reaction and/or diffusion. The interface between the  $\text{BaAl}_2\text{O}_4$  compact and the  $\text{UO}_2$  compact showed no evidence of reaction, but indications of diffusion of  $\text{BaAl}_2\text{O}_4$  into the  $\text{UO}_2$  were noted. The interface between the  $\text{BaAl}_2\text{O}_4$  compact and the UC compact indicated some degree of reaction taking place.

In order to investigate the various reactions in more detail, the mixed compacts (those containing  $\text{BaAl}_2\text{O}_4$  + UC or  $\text{UO}_2$ ) and the barium aluminate compacts were vacuum heat treated for 50 hours at both 1200 and 1400°C. The results of the 50 hour vacuum heat treatments are listed in Table 1.

Table 1  
Weight Loss of  $\text{UO}_2$ - $\text{BaAl}_2\text{O}_4$ , UC- $\text{BaAl}_2\text{O}_4$  and  $\text{BaAl}_2\text{O}_4$   
Compacts After Vacuum Heat Treatment for 50 Hours

Specimen Composition	Weight Loss, Percent	
	1200°C	1400°C
75 w/o UC - 25 w/o $\text{BaAl}_2\text{O}_4$	6.45	22.4
60 w/o $\text{UO}_2$ - 40 w/o $\text{BaAl}_2\text{O}_4$	0.14	0.4
100% $\text{BaAl}_2\text{O}_4$	0.4 to 0.7	1.1 to 2.4

X-ray examination of the samples containing  $\text{UO}_2$  revealed only patterns of  $\text{UO}_2$  and  $\text{BaAl}_2\text{O}_4$  after the 50 hour heat treatment at 1200°C. The results obtained on these samples showed a very sharp pattern for the  $\text{BaAl}_2\text{O}_4$  as compared to the originally prepared  $\text{BaAl}_2\text{O}_4$  powder, apparently resulting from grain growth and homogenization with heat treatment. From the weight loss data and the microstructures, the samples containing  $\text{UO}_2$  appeared most promising from a compatibility standpoint, even though the  $\text{UO}_2$  apparently formed a solid solution with the  $\text{BaAl}_2\text{O}_4$ . The UC on the other hand, was chemically incompatible with the  $\text{BaAl}_2\text{O}_4$ . The structure of the samples containing UC was quite porous and brownish in color suggesting the formation of  $\text{UO}_2$ . The carbon analysis of the compacts dropped from a calculated value of 3.71 w/o to an analysed value of 3.2 w/o after heat treatment. The UC apparently reacted with the  $\text{BaAl}_2\text{O}_4$  to form CO, free barium,  $\text{Al}_2\text{O}_3$ , and  $\text{UO}_2$ . Because of the extensive reactions that took place between the barium aluminate and uranium carbide, this system did not seem worthy of further investigation and was dropped from the program.

## B. BaO-UO<sub>2</sub> SYSTEM

As pointed out above, the barium aluminate and uranium oxide materials appeared to be chemically compatible with one another; only diffusion of BaAl<sub>2</sub>O<sub>4</sub> into UO<sub>2</sub> was evident. Initially the aluminum oxide was added to the barium oxide activator in order to reduce the chemical activity of the BaO in the completed emitters. However, no advantage could be seen for the use of aluminum oxide in emitter materials that contain UO<sub>2</sub>, so the program was shifted in order to concentrate only on the barium oxide-uranium oxide system.

Uranium dioxide has found considerable use as a high temperature reactor fuel; therefore, its physical and chemical properties as well as phase equilibria with other metal oxides have been of major interest. However, only limited information on the BaO-UO<sub>2</sub> system is available, and this has been reported by Lang,<sup>(2)</sup> Furman,<sup>(3)</sup> and Trzebiatowski.<sup>(4)</sup> In the BaO-UO<sub>2</sub> system, the presence of BaUO<sub>3</sub>, Ba<sub>2</sub>UO<sub>4</sub>, Ba<sub>3</sub>UO<sub>5</sub>, BaU<sub>2</sub>O<sub>6</sub> and Ba<sub>2</sub>UO<sub>5</sub> have been reported, although not all have been proven to exist. Lang, et al.<sup>(2)</sup> found the BaO-UO<sub>2</sub> system to resemble the calcium and strontium systems, except that the perovskite-type compound, BaUO<sub>3</sub>, was pseudo-cubic ( $a_c = 4.387 \text{ \AA}$ ) rather than orthorhombic. The solubility of BaO in the UO<sub>2</sub> solid solution structure was estimated to be 25 mole percent at 1800°C. Some evidence for solid solubility of barium oxide in BaUO<sub>3</sub> was also observed. Mixtures of 2BaO:1UO<sub>2</sub> (mole ratio) contained a single-phase cubic perovskite-type solid solution after reaction at 1800°C for one-half hour in argon, as contrasted with 3BaO:1UO<sub>2</sub> mixtures which contained free barium oxide.

Furman<sup>(3)</sup> has also identified the compound BaUO<sub>3</sub> as one product of the reaction between barium oxide and uranium dioxide. He reported the compound as being in the cubic system with  $a_o = 4.37 \text{ \AA}$ , and concluded that barium oxide and uranium dioxide react stoichiometrically to form the true compound BaUO<sub>3</sub>. Trzebiatowski et al.<sup>(4)</sup> indicated that for compositions up to 50 m/o BaO, only UO<sub>2</sub> and BaUO<sub>3</sub> phases exist. He states, that from the lattice constants, no solubility of UO<sub>2</sub> in BaUO<sub>3</sub> or BaO in UO<sub>2</sub> is to be expected. At 50 m/o BaO the compound BaUO<sub>3</sub> is formed with a pseudo-cubic perovskite structure. At higher BaO contents, his work shows a marked solubility of BaO in BaUO<sub>3</sub>. This solution persisted up to 75 m/o BaO.

Based on the above information a tentative phase diagram for the BaO-UO<sub>2</sub> system was constructed. This phase diagram is presented in Fig. 2. The most important aspect of the phase diagram is the formation of barium uranate (BaUO<sub>3</sub>),



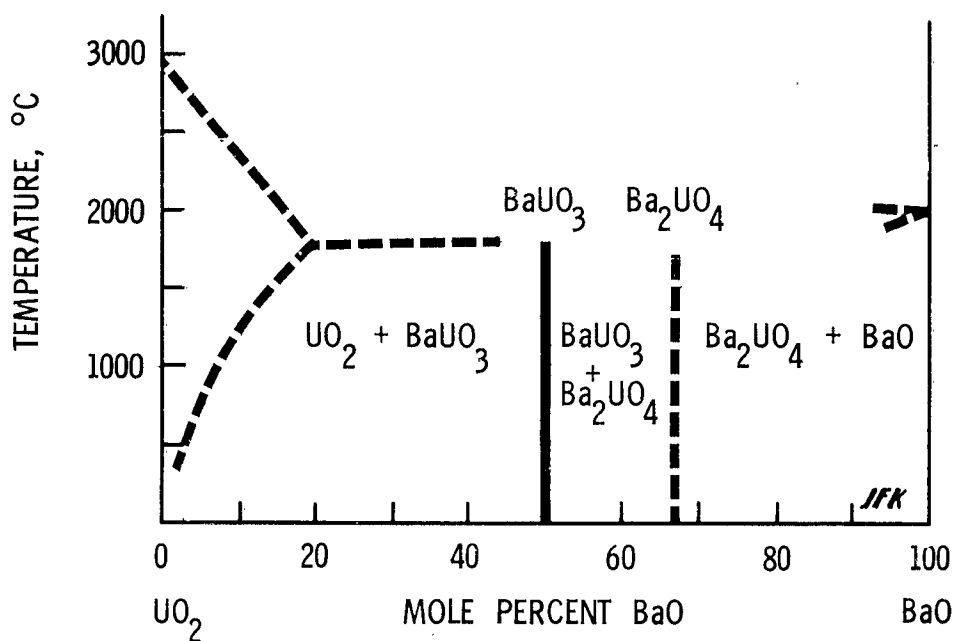


Figure 2 - Tentative phase diagram of the BaO-UO<sub>2</sub> system.

which was reported by all three investigators listed above. The pseudo-cubic perovskite structure for BaUO<sub>3</sub> as discussed above must have the following general atom arrangement.

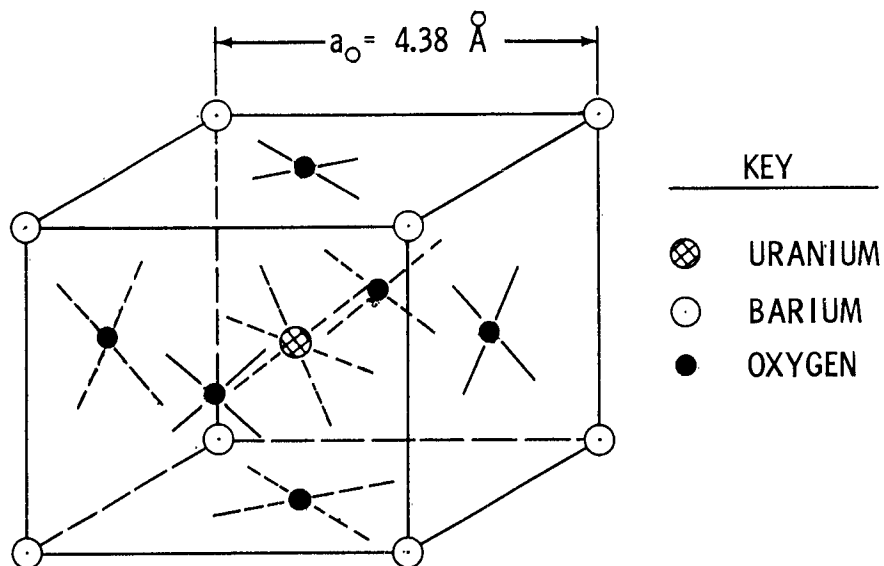


Figure 3 - BaUO<sub>3</sub> perovskite crystal structure.

By the use of the above crystal model the theoretical density for  $\text{BaUO}_3$  was calculated to be

$$\rho = \frac{137 + 238 + 3(16)}{(4.38 \times 10^{-8})^3 \times 6.02 \times 10^{23}} = 8.34 \text{ gm/cc} \quad (1)$$

### C. $\text{BaO-UO}_2$ EMITTER MATERIAL STUDIES

The basic design of the uranium containing emitters consisted of a tungsten or rhenium matrix impregnated with an appropriate barium-uranium oxide mixture. Since the characteristics of the completed emitter depended upon the chemical composition of the oxide, various  $\text{BaO-UO}_2$  mixtures were fabricated and evaluated on the basis of x-ray analysis, microstructure, chemical analysis and evaporation rate.

The various  $\text{BaO-UO}_2$  mixtures were prepared by blending together minus 200 plus 270 mesh  $\text{UO}_2$  powder with  $\text{BaCO}_3$  powder to form the desired oxide compositions. The powders were mixed in a ceramic mortar. A compact of each mixture was green-pressed in a one inch diameter die and inserted into a tungsten lined tantalum boat. The specimens were then sintered in a hydrogen atmosphere for an hour and a half at  $1650^\circ\text{C}$ . Seven blends of  $\text{BaO-UO}_2$ , nominal compositions ranging between 25 and 75 mole percent  $\text{BaO}$ , were fabricated and analyzed for barium and uranium content. The chemical compositions are summarized in Table 2.

Table 2  
Chemical Composition of Various  $\text{BaO-UO}_2$  Samples

Mole % $\text{BaO}$ (Balance $\text{UO}_2$ )		Chemical Composition, w/o	
		Barium	Uranium
Nominal molar composition	25	10.7	77.1
	40	24.0	63.8
	45	27.7	60.0
	50	31.9	55.8
	60	40.0	46.8
	70	48.2	39.6
	75	50.2	34.0

The balance of the chemical composition was predominantly oxygen. The various  $\text{BaO-UO}_2$  samples were selected on the basis of the phase diagram presented in Fig. 2. The approach was to select several compositions from each region of the phase diagram in order to determine the effects of the various  $\text{BaO-UO}_2$  compounds on the evaporation rate and electron emission characteristics of the oxide mixtures.

The various BaO-UO<sub>2</sub> mixtures, that are listed in Table 2, were heat treated for 50 hours at 1200 and 1400°C both as separate samples and as blends containing 25 and 75 volume percent tungsten. X-ray analysis, microstructures and weight loss data were obtained on the various samples.

#### 1. X-Ray Analysis

The various BaO-UO<sub>2</sub> mixtures were submitted for x-ray analysis both prior and after heat treatment. The x-ray analysis of the various oxides after sintering but prior to heat treatment are presented in Table 3.

Table 3

X-Ray Analysis of the BaO-UO<sub>2</sub> System

Mole % BaO	Phases	Pattern Strength	Lattice Content, a <sub>o</sub>
25	BaUO <sub>3</sub>	Weak	4.36 Å
	UO <sub>2</sub>	Strong	
40	BaUO <sub>3</sub>	Strong	4.33 Å
	UO <sub>2</sub>	Medium	
45	BaUO <sub>3</sub>	Strong	4.36 Å
	UO <sub>2</sub>	Medium	
50	BaUO <sub>3</sub>	Strong	4.36 Å
	UO <sub>2</sub>	Very weak	
60	BaUO <sub>3</sub>	Strong	4.38 Å
	'X'	Weak	
70	'Y'	Strong	8.86 Å
75	'Y'	Strong	8.88 Å

The x-ray diffraction patterns of the mixtures that contained less than 50 m/o BaO showed lines for both BaUO<sub>3</sub> and UO<sub>2</sub>. The diffraction lines revealed that the compound BaUO<sub>3</sub> had a lattice constant of a<sub>o</sub> = 4.36 Å which appeared to be in agreement with the 4.387 Å value reported by Lang.<sup>(2)</sup> The slight disagreement with Lang's value apparently was a result of saturation of the BaUO<sub>3</sub> structure with UO<sub>2</sub>.

The x-ray analysis of the mixtures containing more than 50 m/o BaO indicated basically two types of structures. These were defined as 'X' and 'Y'. The 'Y' phase had a complex face-centered cubic structure that required a double cell arrangement in order to account for all of the observed lines. Chemical analysis of the 'Y' phase indicated that it had a composition closely to that of Ba<sub>2</sub>UO<sub>4</sub>. The 'X' phase was of an intermediate composition between BaUO<sub>3</sub> and the 'Y' phase.

In general, the observed x-ray diffraction lattice constants of the seven blends of  $\text{BaO-UO}_2$  increased with increased BaO content. However the lattice constants were lower than the values reported by Trzebiatowski.<sup>(4)</sup> It was believed that the lower values were due to deviations from the stoichiometric compositions and from oxidation obtained during preparation of the x-ray samples.

X-ray analyses on the  $\text{BaO-UO}_2$  mixtures were also obtained after the 50 hour heat treatments at 1200 and 1400°C. The  $\text{BaUO}_3$  phase observed in these samples was the same as previously reported. The 'X' phase, which was also detected after 50 hours at 1200°C, had a tetragonal structure with  $a_o = 5.71 \text{ \AA}$  and  $c_o = 5.58 \text{ \AA}$ . However, there was some indication that the 'X' phase resulted from a blend inhomogeneity since it was not detected after the 1400°C heat treatment. The 'Y' phase was observed for both the 70 and 75 mole percent BaO mixtures after the 1200 and 1400°C heat treatments and had the same structure as previously reported. The 'Y' phase face-centered cubic structure possibly resulted from the substitution of barium atoms for some of the uranium atoms in the crystal lattice and thus required a doubling of the lattice parameters. Chemical analysis again indicated that the 'Y' phase corresponded to that of  $\text{Ba}_2\text{UO}_4$ . A very weak pattern of a new phase was observed for the 75 mole percent BaO mixture after both heat treatments and was designated as phase 'Z'. This phase appeared to be hexagonal in structure and its formation was believed to result from a reaction between excess BaO and the 'Y' phase.

## 2. Microstructure Analysis

Samples of the various oxide materials both separately and combined with tungsten were formed into dense compacts by gas-pressure bonding. This was accomplished by green-pressing the various powder mixtures into pellets, loading the pellets into niobium tubes, and gas-pressure bonding at 1500°C for 3 hours under a helium gas pressure of 10,000 psi. The samples that contained tungsten were prepared at two composition levels, namely; 25 v/o oxide + 75 v/o tungsten and 75 v/o oxide + 25 v/o tungsten. After pressure bonding the niobium cladding was removed from the various samples. The samples were then examined by metallographic techniques in order to determine their degree of homogenization.

Typical photomicrographs of two emitter materials are shown in Figs. 4 and 5. In Fig. 4 the specimens contained nominally 25 v/o tungsten and 75 v/o oxide, where the oxide composition was 45 m/o BaO and 55 m/o  $\text{UO}_2$ . In this figure the unreacted spherical  $\text{UO}_2$  particles are surrounded by the dark gray solid solution of  $\text{BaUO}_3$ . The white matrix is the tungsten. Although the  $\text{UO}_2$  has remained

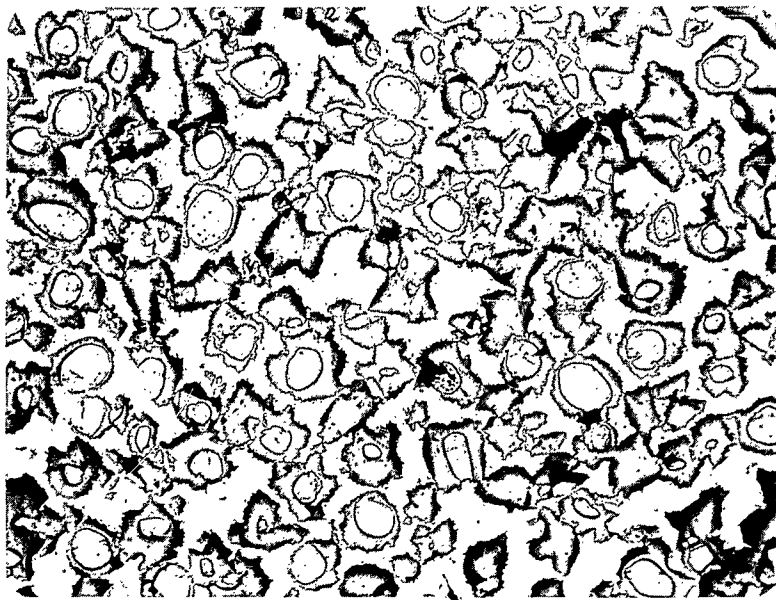


Figure 4 - Nominal 25 v/o W and 75 v/o (45 m/o BaO - 55 m/o  $\text{UO}_2$ ) - 100X



Figure 5 - Nominal 25 v/o W and 75 v/o (60 m/o BaO - 40 m/o  $\text{UO}_2$ ) - 100X

spherical, the reaction zone appears to be homogeneous indicating that the reaction between the  $\text{UO}_2$  and  $\text{BaO}$  has gone to completion.

Figure 5 shows the single gray  $\text{BaUO}_3$  phase of the 60 m/o  $\text{BaO}$  - 40 m/o  $\text{UO}_2$  material dispersed in a white matrix of tungsten. As before this specimen contained nominally 25 v/o tungsten and 75 v/o oxide. It is interesting to note from Fig. 5 that the shape of the  $\text{BaUO}_3$  particles is quite irregular, as compared to the initial oxide blend in which spherical  $\text{UO}_2$  powder was used.

As the barium oxide content of the various specimens was increased, the microstructures showed a diminishing amount of unreacted spherical  $\text{UO}_2$  and an increasing amount of gray  $\text{BaUO}_3$  phase. Above 50 m/o  $\text{BaO}$  the microstructures indicated a single phase structure of either  $\text{BaUO}_3$  or  $\text{Ba}_2\text{UO}_4$  with the excess barium oxide being in solid solution.

Based upon the above x-ray analysis and microstructure analysis the following general comments on the  $\text{BaO}$ - $\text{UO}_2$  system can be established.

- (1) There are at least two ( $\text{BaUO}_3$  and  $\text{Ba}_2\text{UO}_4$ ) and possibly as many as five Ba-U-O compounds.
  - (2)  $\text{BaUO}_3$  has a perovskite-type structure and has been detected over the nominal composition range from 25 to 60 mole percent  $\text{BaO}$ .
  - (3)  $\text{Ba}_2\text{UO}_4$  has a face centered cubic structure and has been detected over the nominal composition range of 70 - 75 mole percent  $\text{BaO}$ .
  - (4) There is limited solid solubility of  $\text{BaO}$  in  $\text{UO}_2$ .
  - (5) There is limited solid solubility of  $\text{UO}_2$  in  $\text{BaUO}_3$ .
  - (6) There is extensive solubility of  $\text{BaO}$  in  $\text{BaUO}_3$  and  $\text{Ba}_2\text{UO}_4$ .
3. Evaporation Rate Data

Densified samples of the various oxide materials both separately and combined with tungsten were subjected to vacuum heat treatments for 50 hours at both 1200 and 1400°C. The weight loss data of the various samples are summarized in Table 4.

Table 4

Weight Loss Data Obtained - 50 Hours at 1200 and 1400°C

Mole % $\text{BaO}$ ( $\text{Ba}$ $\text{UO}_2$ )	Percent Weight Loss of Total Specimen					
	1200°C			1400°C		
	Oxide	25 v/o W*	75 v/o W*	Oxide	25 v/o W*	75 v/o W*
25	0.34	0.4	0.14	1.2	0.51	0.26
40	0.61	0.52	0.38	0.15	2.2	0.71
50	0.85	0.74	0.36	-	3.8	1.3
60	2.6	1.0	0.51	5.1	2.3	0.75
70	3.1	0.7	0.43	-	2.7	0.99
75	1.5	1.7	0.4	8.2	3.6	0.4

\* - Balance oxide

The weight loss data presented in Table 4 are based on a limited number of tests so that the absolute value recorded for any single point may contain some degree of error, but the general trends indicated are real. In general, the weight loss based on the total weight of the specimen increased with an increase in temperature and decreased with an increase in volume percent of tungsten. An increase in mole percent BaO generally increased the total weight loss. When relating the weight loss to the oxide content only, ignoring the tungsten content, there was a higher percent loss with increased temperature, increased volume loading of tungsten and increased barium oxide content.

In reviewing the above x-ray data and microstructure analysis, it was noted that for materials containing less than fifty mole percent barium oxide, the BaO was combined with the  $\text{UO}_2$  to form  $\text{BaUO}_3$  while the excess uranium oxide was present as  $\text{UO}_2$ . However for materials containing barium oxide in excess of fifty mole percent there was no free  $\text{UO}_2$  and the excess barium oxide was tied up as higher barium - uranium compounds. In reviewing the weight loss data presented in Table 4 on this basis, it was noted that the evaporation rate showed a substantial increase above 50 m/o BaO.

This change in evaporation rate can possibly be explained in the following manner. If it is assumed that the weight loss is due mainly to the evaporation of barium oxide, then at compositions containing less than 50 m/o BaO the barium oxide will have a lower effective evaporation rate than will free BaO because it is held in the compound  $\text{BaUO}_3$ . On the other hand, materials having compositions greater than 50 m/o BaO can release free BaO quite readily even though BaO- $\text{UO}_2$  compounds are indicated. For example the reaction  $\text{Ba}_2\text{UO}_4 = 1 \text{ BaO} + \text{BaUO}_3$  can release free BaO very readily where this free BaO will exert a higher vapor pressure than can BaO as tied up in  $\text{BaUO}_3$ .

When tungsten was added to the system the evaporation rate of barium from the emitter material was increased. This resulted from the fact that the tungsten reduced the barium oxide to free barium which in turn exerted a higher vapor pressure than did the BaO. This effect can be seen from the data presented in Table 4 if the percent weight loss is based only on the barium oxide content of the sample.

Figure 6 shows the relationship between weight percent and mole percent of barium oxide in a sample with volume percent tungsten as a parameter. Also included in Fig. 6 are the theoretical densities of the various oxide materials. The curves presented in Fig. 6 were calculated on the basis of the theoretical density for the various materials.

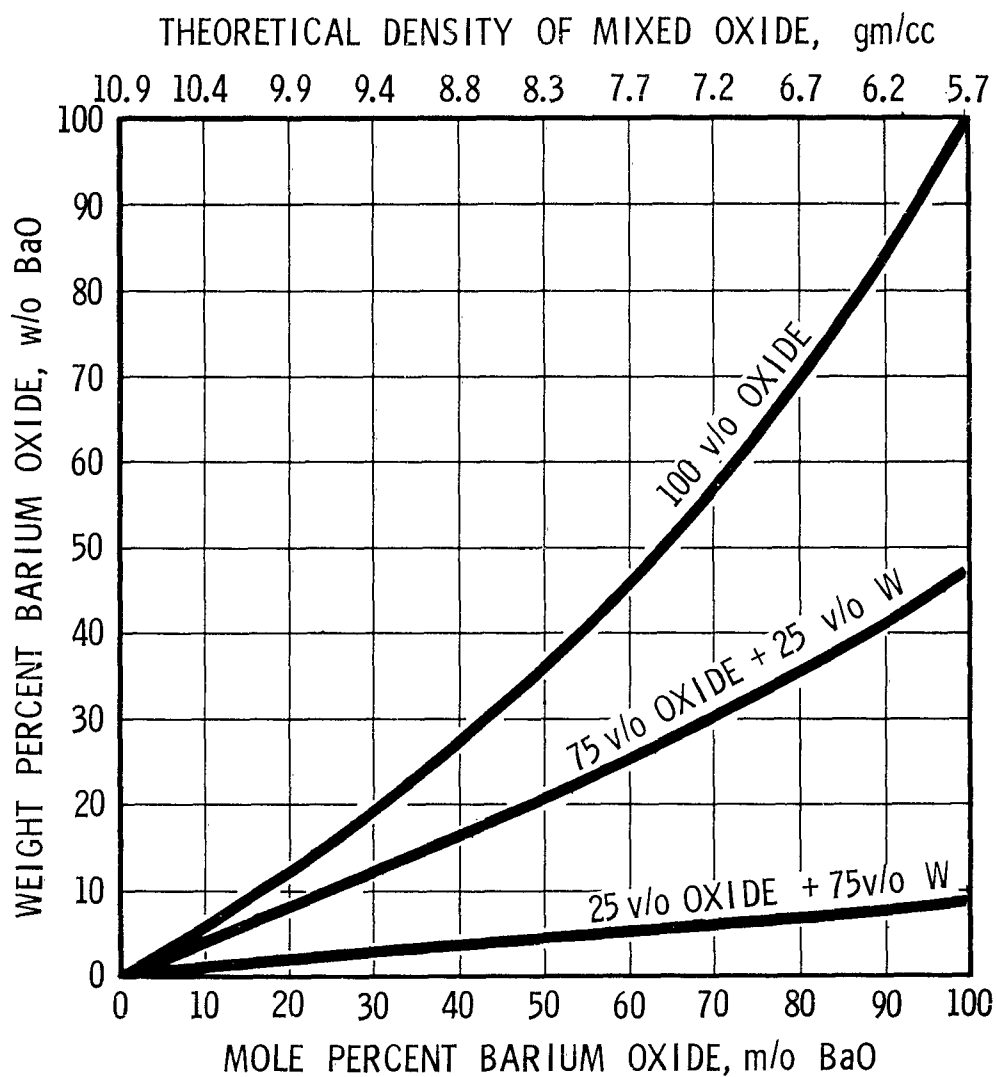


Figure 6 - Conversion of mole percent to weight percent barium oxide for BaO-UO<sub>2</sub>-W systems.

By the use of Fig. 6, the weight loss data presented in Table 4 were calculated in terms of the barium oxide content of the samples. These data are presented in Table 5.



Table 5  
Weight Percent Loss Based on Barium Oxide Content Only  
50 Hours at 1200°C

<u>Mole % BaO</u>	<u>Oxide</u>	<u>Oxide + 25 v/o W</u>	<u>Oxide + 75 v/o W</u>
25	2.1	4.2	7.0
40	2.3	3.2	10.8
50	2.4	3.7	8.0
60	5.6	4.1	10.0
70	5.5	2.3	7.2
75	2.4	5.3	5.7

The above data again show only general trends, since the absolute values are not exact due to inaccuracies in theoretical density measurements.

In examining the data present in Table 5 it was noted that the samples containing tungsten lost a greater percent of their barium content than did samples which did not contain tungsten. This may indicate that the tungsten is definitely reducing the barium oxide to free barium. At the temperatures investigated, free barium would evaporate from the specimens at a faster rate than would barium oxide thus accounting for the higher weight loss. It should be pointed out, however, that the above weight loss data are based on only one test at each composition which does not necessarily present adequate information for drawing definite conclusions.

In order to investigate the evaporation rate of the BaO-UO<sub>2</sub>-W system in more detail, dense cermet compacts representing the three major regions of the BaO-UO<sub>2</sub> phase diagram (Fig. 2) were fabricated and vacuum heat treated at 1200°C. Weight loss data were obtained from the samples after 5, 50, 133, 200 and 308 hours. The compositions of the various cermet samples are listed in Table 6.

Table 6  
Chemical Composition of Evaporation Rate Samples

<u>Specimen Number</u>	<u>Chemical Composition</u>
7545	75 v/o (45 m/o BaO - 55 m/o UO <sub>2</sub> ) - 25 v/o W
7560	75 v/o (60 m/o BaO - 40 m/o UO <sub>2</sub> ) - 25 v/o W
2560	25 v/o (60 m/o BaO - 40 m/o UO <sub>2</sub> ) - 75 v/o W
7570	75 v/o (70 m/o BaO - 30 m/o UO <sub>2</sub> ) - 25 v/o W

The specimen numbers, as listed in Table 6, are a code to the compositions. The first two numbers indicate the volume percent loading of oxide in the material, while the last two numbers indicate the mole percent of barium oxide in the oxide portion. For example, the number 1540 would indicate 15 v/o oxide (85 v/o metal matrix) with the oxide containing 40 m/o BaO (60 m/o UO<sub>2</sub>).

Two sizes of particles were used in the preparation of the various samples. In one set of samples the oxide particles were 100 mesh while in the other set the oxide was reduced to 325 mesh. In both cases the tungsten powder was 325 mesh. The results of the weight loss data based on the total weight of the specimen are presented in Fig. 7.

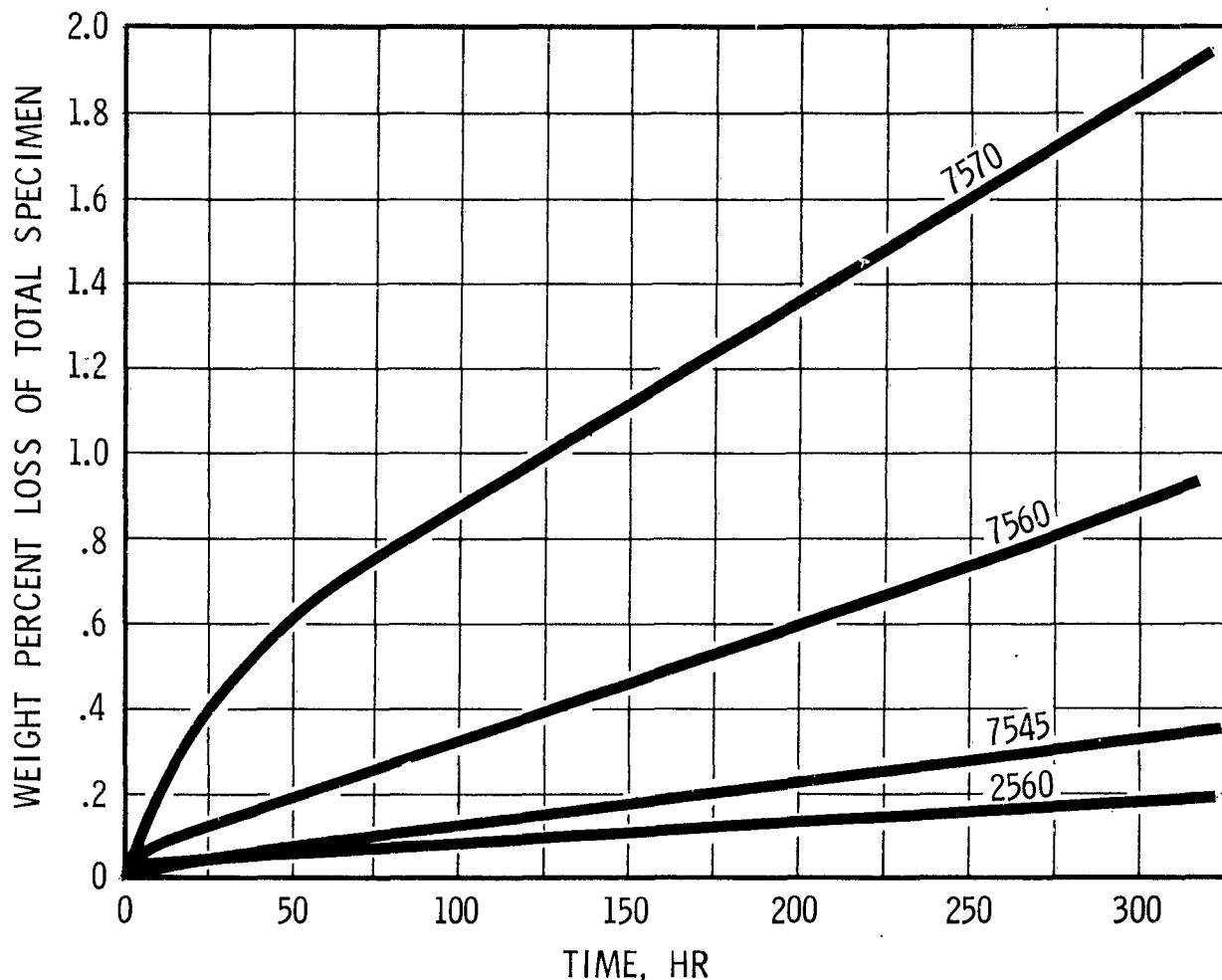


Figure 7 - Weight loss of the various BaO-UO<sub>2</sub>-W specimens that are listed in Table 6, measured at 1200°C in a vacuum.

In general, the weight loss when based on the total weight of the specimen increased linearly with time in excess of 50 hours. The increase in mole percent BaO increased the total weight loss provided that the volume percent of tungsten remained constant. No effect of the oxide particle size on the total weight loss could be distinguished.

When relating the weight loss to the oxide content only, neglecting the tungsten content, there was higher percent loss with increased time and increased BaO content. Again, the weight loss was nearly linear with time in excess of 50 hours. Also the higher tungsten content (2560 as opposed to 7560) resulted in a higher percent weight loss when expressing the weight loss in terms of the oxide content only. This again indicates the importance of the tungsten in reducing the barium oxide to free barium atoms.

#### 4. Density Determination

Several of the dense cermet compacts that were fabricated for the evaporation rate studies were subjected to detailed density measurements. The results of these investigations are summarized in Table 7.

Table 7

Specimen No.	Density of Emitter Cores		% T.D.*
	Density, gm/cc		
	Theoretical	Measured	
7575	11.82	10.64	90
2575	17.4	15.3	88
7525	13.05	12.39	95
2525	17.70	14.2	80

\* % T.D. - Percent of Theoretical Density

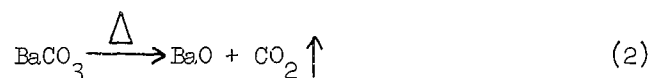
The theoretical densities of the various cermet compacts presented in Table 7 were calculated by using the theoretical oxide densities listed in Fig. 6 and a tungsten density of 19.3 gm/cc. The density for the nominal 25 m/o BaO - 75 m/o  $UO_2$  mixture was calculated to be 9.74 gm/cc while the density for the nominal 75 m/o BaO - 25 m/o  $UO_2$  mixture was calculated to be 7.61 gm/cc. These values are corrected for chemical composition. From the data presented in Table 7 it can be seen that the gas-pressure bonding process can be used to produce cermet emitters with densities in the range of 80 - 95 percent of theoretical. Analysis of the microstructures indicated that the majority of the specimens were in excess of 90% T.D.

The theoretical density of the various BaO- $UO_2$  mixtures are shown at the top of Fig. 6. These values were calculated on the assumption that the mixed oxides formed ideal solid solutions. It should be noted that there is close agreement between the density for the 50 m/o BaO - 50 m/o  $UO_2$  composition as presented in Fig. 6 and the value calculated from the lattice parameters as presented in Eq. 1. The two densities are 8.3 gm/cc and 8.34 gm/cc respectively.

## 5. Thermodynamics of the Barium Oxide - Uranium Oxide System

It is of major importance that some preliminary insight be gained into the thermodynamics of the barium oxide - uranium oxide system, for this insight will aid in the evaluation of the material studies presented above.

As stated before, the barium oxide - uranium oxide system was prepared by blending together  $\text{BaCO}_3$  and  $\text{UO}_2$ . The mixture was then heated in a hydrogen atmosphere until it fused. During this process the barium carbonate decomposed into barium oxide and carbon dioxide by the reaction

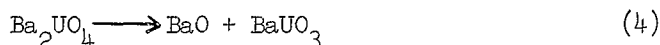


The resulting barium oxide would then combine with the uranium dioxide to form the various  $\text{BaO-UO}_2$  compounds. After cooling, the fused mass was reduced to a fine powder and then mixed with the appropriate matrix metal. The final powder blends were then formed into dense cermet compacts by gas-pressure bonding for 3 hours at  $1500^\circ\text{C}$  under a helium gas pressure of 10,000 psi.

Under actual operating conditions the barium oxide reacts with the metal matrix for the formation of free barium, namely



where M is the matrix metal. The free barium then migrates to the surface of the emitter where it produces the desired electron emission characteristics. As the barium oxide is consumed (by reaction and evaporation), the higher  $\text{BaO-UO}_2$  compounds can supply the additional barium oxide as follows



Also, as pointed out above, both  $\text{BaUO}_3$  and  $\text{Ba}_2\text{UO}_4$  can hold excess BaO in solid solution which in turn can readily be released for barium production.

The useful life of an emitter depends upon the rate of evaporation of barium from the emitter which in turn is related to the pressure of barium vapor in equilibrium with the barium compound and matrix material. If the products are gaseous, the equilibrium pressure can be derived from the free energy of the reaction as follows:

$$\Delta F = R T \ln P_{\text{atm}} \quad (5)$$

where  $\Delta F$  is the change in free energy occurring in the reaction, R is the gas constant and T is the absolute temperature at which the reaction is taking place. The rates of evaporation can be calculated from the equilibrium pressure by the equation

$$Q = 5.83 \times 10^{-2} P(\text{M/T})^{1/2} \quad (6)$$

where  $Q$  is the evaporation rate in  $\text{gm/cm}^2\text{-sec}$ ,  $P$  is the pressure in Torr (mm of Hg) and  $M$  is the molecular weight of the substance in question.

At this point, some preliminary thermodynamic calculations for various emitter material combinations will indicate the importance of chemical compatibility. In order to show the basis for these calculations, the free energies of formation for the various emitter material components as a function of temperature are listed in Table 8.

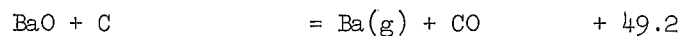
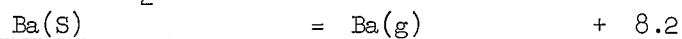
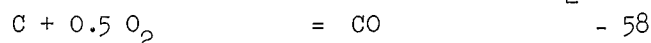
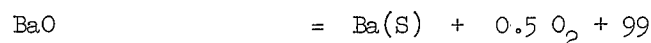
Table 8  
Free Energy of Formation ( $-\Delta F$ ) K cal/mole  
Temperature °K

Material	300	500	1000	1500	2000	Reference
BaO	126	121	109	99	86	5
CO	33	37	48	58	69	5
UC	18.9	18.2	16.3	14.4	12.6	6
UO <sub>2</sub>	246	238	218	198	177	5
WO <sub>3</sub>	182	169	140	111	84	7
Ba*(g)		-28	-17	-8.2		8

$$*\text{Ba}(\text{S}) = \text{Ba}(\text{g}) + \Delta F_V$$

The equilibrium barium vapor pressure resulting from various reactions between barium oxide and carbon, uranium carbide and tungsten were calculated using the free energy data listed above. The details of these calculations are presented below.

Case 1. The vapor pressure of barium produced when a mixture of barium oxide and carbon is heated to 1500°K.

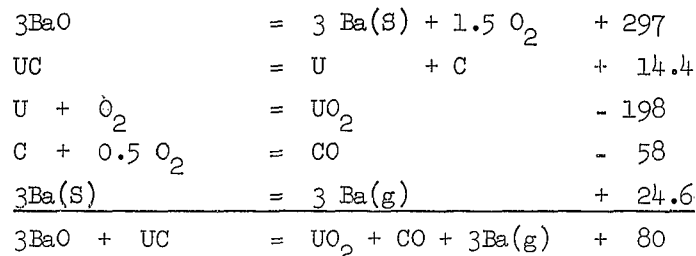


$$\Delta F = -R T \log P_{\text{Ba}} P_{\text{CO}} = -R T \log P_{\text{Ba}}^2$$

$$\log P_{\text{Ba}} = -3.56$$

$$P_{\text{Ba}} = P_{\text{CO}} = 2.8 \times 10^{-4} \text{ atm} = 2.1 \times 10^{-1} \text{ Torr}$$

Case 2. The vapor pressure of barium produced when a mixture of barium oxide and uranium carbide is heated to 1500°K.



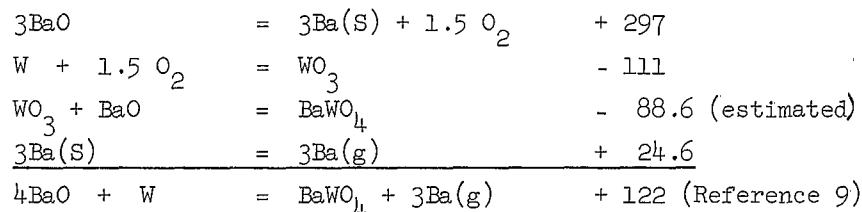
$$\Delta F = - R T \log P_{\text{CO}} P_{\text{Ba}}^3 = - R T \log 27 P_{\text{CO}}^4$$

$$\log P_{\text{CO}} = - 3.25$$

$$P_{\text{CO}} = 5.6 \times 10^{-4} \text{ atm} = 4.25 \times 10^{-1} \text{ Torr}$$

$$P_{\text{Ba}} = 3 P_{\text{CO}} \approx 1.3 \text{ Torr}$$

Case 3. The vapor pressure of barium produced when a mixture of barium oxide and tungsten is heated to 1500°K.



$$\Delta F = - R T \log P_{\text{Ba}}^3$$

$$\log P_{\text{Ba}} = - 5.9$$

$$P_{\text{Ba}} = 1.2 \times 10^{-6} \text{ atm} = 9.1 \times 10^{-4} \text{ Torr}$$

The calculated equilibrium barium vapor pressure for the various reactions between barium oxide and carbon, uranium carbide and tungsten are summarized below in Table 9. Also included in Table 9 are the barium evaporation rates in gm/cm<sup>2</sup>-hr as calculated by Eq. 6.

Table 9

Calculated Barium Vapor Pressure and Evaporation Rate for Various BaO Systems at 1500°K (1227°C)

System	Pressure Torr	Evaporation Rate gm/cm <sup>2</sup> - hr
BaO + W	$9.1 \times 10^{-4}$	$5.8 \times 10^{-2}$
BaO + C	$2.1 \times 10^{-1}$	15
BaO + UC	1.3	83

It should be pointed out that the above calculations assume ideal reactions between the various components. In actual practice, however, the various reactions may become diffusion controlled, thus the evaporation rates listed in Table 9 will represent the upper limits for the various systems. On this basis, the above preliminary calculations indicate that BaO containing emitters will have a very short lifetime when the matrix material contains carbon or uranium carbide. Thus the barium-uranium emitters should be designed around the BaO-UO<sub>2</sub>-W or Re systems. These calculations are in agreement with the compatibility studies listed in the previous sections.

The preceding discussion was mainly concerned with the rates of reduction of BaO by various matrix materials. The question now arises as to the extent of alteration of the reducing power of the matrix material when the barium oxide is diluted with uranium dioxide, because the addition of UO<sub>2</sub> to the barium oxide system can greatly affect the thermodynamics of the resulting emitter materials.

The thermodynamics of the BaO-UO<sub>2</sub>-W systems cannot readily be calculated because the free energy of formation of the various BaO-UO<sub>2</sub> compounds are not known. However, information from the weight loss experiments can be used to supplement the thermodynamic calculations. As pointed out in the section on the evaporation rate studies, the evaporation rates appeared to level off after 50 hours. On this basis, the weight loss data presented in Fig. 7 have been evaluated in terms of the evaporation rate expressed in gm/cm<sup>2</sup>-hr. These data, from the straight line portion of the curves from Fig. 7, are presented in Table 10. Also included in Table 10 are the emission current densities calculated for the various emitters at 1200°C. The emission current densities for these various materials are discussed in more detail in Section III of this report.

Table 10  
Evaporation Rates and Emission Current Densities  
of BaO-UO<sub>2</sub>-W Specimens at 1200°C

Specimen Number	Evaporation Rate gm/cm <sup>2</sup> -hr	Emission Current Density amp/cm <sup>2</sup>
7570	$2.5 \times 10^{-5}$	20.2 (extrapolated)
7560	$9 \times 10^{-6}$	8.9 (measured)
7545	$4 \times 10^{-6}$	2.7 (measured)
2560	$3 \times 10^{-6}$	0.18(measured)

Analysis of the data presented in Table 10 indicates that the barium evaporation rates for the various BaO-UO<sub>2</sub>-W samples were less than 1/1,000 of that calculated for the BaO-W system as listed in Table 9. This was possibly due to

the formation of various  $\text{BaO-UO}_2$  compounds which, in turn, would reduce the chemical activity of the BaO and thus make it more difficult for the tungsten to produce free barium. The reduced barium evaporation rates, due to the formation of  $\text{BaO-UO}_2$  compounds, are in general agreement with calculations for the  $\text{BaO-Al}_2\text{O}_3$  system as presented by Hughes et al.<sup>(10)</sup> Hughes showed that the  $\text{Ba}_3\text{Al}_2\text{O}_6$ -W system had barium evaporation rates that were about 160 times lower than those calculated for the BaO-W system. Because of the reduced barium evaporation rates and thus longer operating life, tribarium aluminate was selected as the barium source in the Philips impregnated cathode emitters.

The relationship between the evaporation rate and emission current density data presented in Table 10 indicate that as the evaporation rate increases the emission current density also increases. This is in agreement with data presented by Brodie.<sup>(11)</sup> For example, Brodie shows that an 'L' cathode containing BaO-SrO has an emission current density of  $20 \text{ amp/cm}^2$  and a barium evaporation rate of  $1 \times 10^{-5} \text{ gm/cm}^2\text{-hr}$ . This is in very good agreement with the data presented in Table 10 for the 7570 and 7560 specimens.

The above thermodynamic calculations indicate that the  $\text{BaO-UO}_2$ -W emitter materials have evaporation rates that are comparable to the  $\text{BaO-Al}_2\text{O}_3$ -W materials that are presently employed in the Philips impregnated cathode emitters.

#### D. EMITTER SAMPLES

In actual emitters the rate of escape of barium is not only determined by the chemical properties of the constituents, but also by the porosity of the matrix material. Thus thermodynamic calculations can only aid in the general evaluation of the emitter materials. In order to establish the exact emission characteristics of the various emitter materials, actual samples must be fabricated and tested.

Densified cermets of the various  $\text{BaO-UO}_2$ -W materials as described in the previous sections were machined and loaded into tantalum support sleeves for emission studies. The tantalum support sleeves, as shown in detail in Fig. 8, were outgassed in a vacuum for 30 minutes at  $1700^\circ\text{C}$  prior to loading. After loading, the emitter cores were ground on 400 grip paper to level the surface. The cores were kept intact by slightly crimping the edges of the tantalum support sleeves.



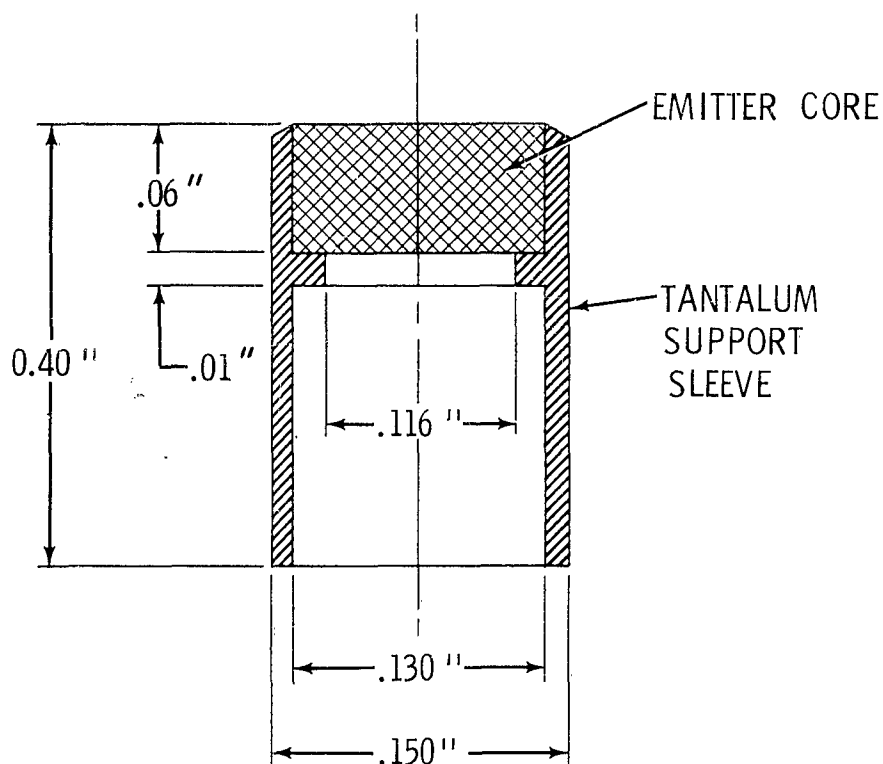


Figure 8 - Tantalum support sleeve showing emitter core.

The various BaO-UO<sub>2</sub> containing samples that have been fabricated for emission testing are listed in Table 11. Both the mole percent of BaO and UO<sub>2</sub> as well as the volume percent metal in the cermet compacts are listed. Those samples marked with the asterisk were prepared with two sizes of oxide particles namely 100 mesh and 325 mesh.

Table 11  
Composition of BaO-UO<sub>2</sub> Emitter Samples

Emitter Number	v/o Oxide	m/o BaO	m/o UO <sub>2</sub>	v/o Metal	w/o BaO in Compact
7575	75	75	25	25 W	33
2575	25	75	25	75 W	7
7525	75	25	75	25 W	9
2525	25	25	75	75 W	2
7545*	75	45	55	25 W	18
7560*	75	60	40	25 W	25
7570*	75	70	30	25 W	30
2560*	25	60	40	75 W	5
7575 R	75	75	25	25 Re	31
2575 R	25	75	25	75 Re	6
7525 R	75	25	75	25 Re	9
2525 R	25	25	75	75 Re	2

From the above table it can be noted that emitter samples containing both tungsten and rhenium matrices were fabricated. The major effort was directed toward the development of tungsten containing emitters as presented in the previous sections. However, x-ray analysis and evaporation rate data obtained on the rhenium containing emitters indicated that the data obtained on the BaO-UO<sub>2</sub>-W system were also applicable to the BaO-UO<sub>2</sub>-Re system.

### III. EMISSION STUDIES

In order to determine the influence of chemical composition on electron emission, the various samples listed in Table 11 were tested by using a high field technique for finding the work function and other emission parameters. This testing was accomplished on special equipment that was specifically designed and fabricated for this project.

#### A. APPARATUS

Figure 9 shows the overall view of the equipment used in processing and testing the emitters. This included a Tektronix 555 scope, camera, pulser, vacuum system, accessory power supply rack, strip recorder and oven power supply. The various components are discussed in detail below.

##### 1. Vacuum System

Two primary aspects were desired in the vacuum station for performing the required experiments, namely; (1) it was of paramount importance that the ultimate pressure of the station be  $10^{-8}$  Torr (mm of Hg) or better in order to maintain clean surfaces on the emitters for reliable and reproducible data, and (2) it was important to be able to readily change from one emitter to another without involving considerable time and effort since many types of emitters were to be tested. Both of these requirements were satisfied in the design of the vacuum system.

The general arrangement of the vacuum system is shown in the center of Fig. 9 along with the supporting test equipment. The pumping system consisted of a fore pump, oil diffusion pump and a liquid nitrogen cold trap all of which were mounted below the surface of the table. The manifold and connecting tubing to the three tubes were located above the table top. A sketch showing the arrangement of the vacuum system components in more detail is presented in Fig. 10.



Figure 9 - Processing and testing equipment used for emission studies.

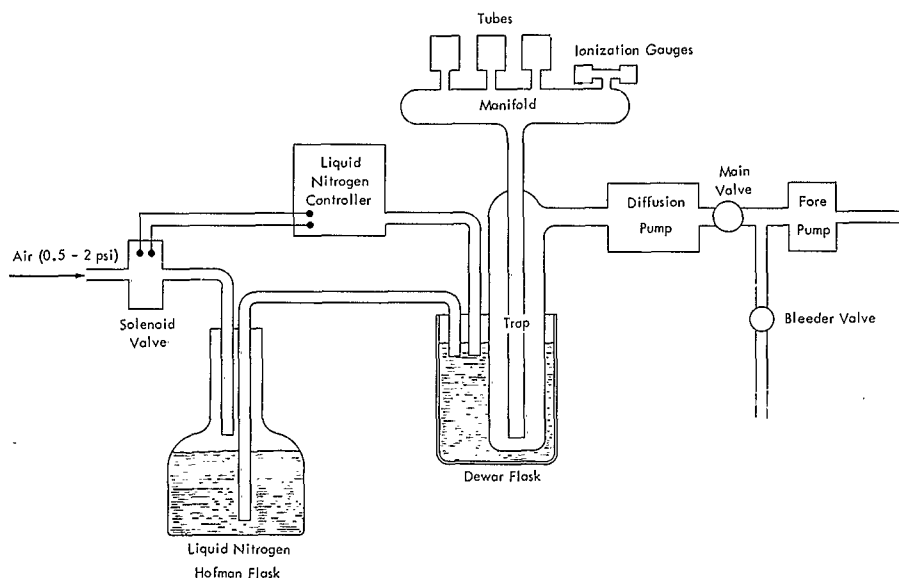


Figure 10 - Sketch of vacuum system.

a. Pumps

The fore pump was a Welch Duo-Seal No. 1405 B with a free air capacity of 58 liters per minute and an ultimate vacuum of  $10^{-4}$  Torr. The diffusion pump was an oil (octoil) CEC type MCF-60 with an ultimate vacuum capability of  $4 \times 10^{-7}$  Torr and having a pumping speed of 68 liters per second at a pressure of  $10^{-3}$  Torr. Later tests using Dow Corning No. 705 silicone diffusion pump fluid indicated that improved pumping speeds could be obtained with the silicone fluid.

b. Liquid Nitrogen Trap

In order to obtain a fast cycling system with a good ultimate pressure, a liquid nitrogen trap was incorporated in the vacuum system between the experimental tubes and the diffusion pump. This trap served two purposes: (1) it reduced the back diffusion of oil from the diffusion pump into the manifold thus aiding in the maintenance of clean emitter surfaces and (2) it serves as an additional pump in the system, trapping out vapors that condense at temperatures above  $-196^{\circ}\text{C}$ . The result of this latter aspect made it possible to obtain pressures on the  $10^{-9}$  Torr scale with a majority of the measurements taken at a pressure of  $2 \times 10^{-9}$  Torr, as recorded by a Bayard-Alpert ionization gauge.

The trap had a large pumping speed due to its 4 in. diameter outside container where the vapors were condensed. In this respect, a one square inch of surface

area at liquid nitrogen temperature will have a pumping speed of approximately 100 liters per second at a pressure of  $10^{-6}$  Torr.

The inside tube was 2 in. in diameter thus allowing ample cross sectional area for the flow of gas from the manifold to the diffusion pump. The trap was constructed of stainless steel with all joints made by heliarc welding. A Ultek type 2 in. high vacuum flange<sup>(12)</sup> was welded to the output end of the trap in order that it could be connected to the diffusion pump by means of a stainless steel elbow. The vacuum seal to the diffusion pump was accomplished by a "Viton A" O ring while a copper gasket was employed at the trap end of the elbow. The input end of the trap was welded to Kovar which was in turn joined to pyrex glass through a graded glass seal. All metal parts were hydrogen fired at 1200°C prior to assembly. This reduced the 'out gassing' tendency of the metal.

A Dewar flask was used on the trap during the processing of the emitters. In order to maintain the desired level of liquid nitrogen in the Dewar flask an automatic liquid nitrogen level controller<sup>(13)</sup> was employed. A 25 liter liquid nitrogen Hofman flask served as a sufficient reservoir for a period of 24 hours unattended, when used in conjunction with this nitrogen controller.

A bakeout oven was also designed to fit over the trap. This oven, which was used during the bakeout of the vacuum system, was capable of heating the trap to the normal operating temperature of 450°C.

One main valve was located between the diffusion pump and fore pump in order to permit shutting down the pumps and yet allowing a low pressure to be maintained on the high vacuum side. This feature aided in keeping the tubes clean and dry during short intervals such as weekends, etc. before reloading the tubes for additional tests. In conjunction with this, a Drierite tube was inserted in the bleeder line along with a valve, in order to dry the air when the system was opened to atmospheric pressure for reloading the tubes.

#### c. Vacuum Manifold

The high vacuum glass manifold along with ionization gauges, tubes and support stand is shown in more detail in Fig. 11. Each of the three tubes may be observed connected to the main manifold by a right angle double flexible glass bellows. This feature enhanced the possibility that the glass would remain integral when removing or inserting the demountable bases in each of the three tubes. It also provided for thermal expansion differentials during bakeout. With this arrangement three tubes could be processed and tested simultaneously.

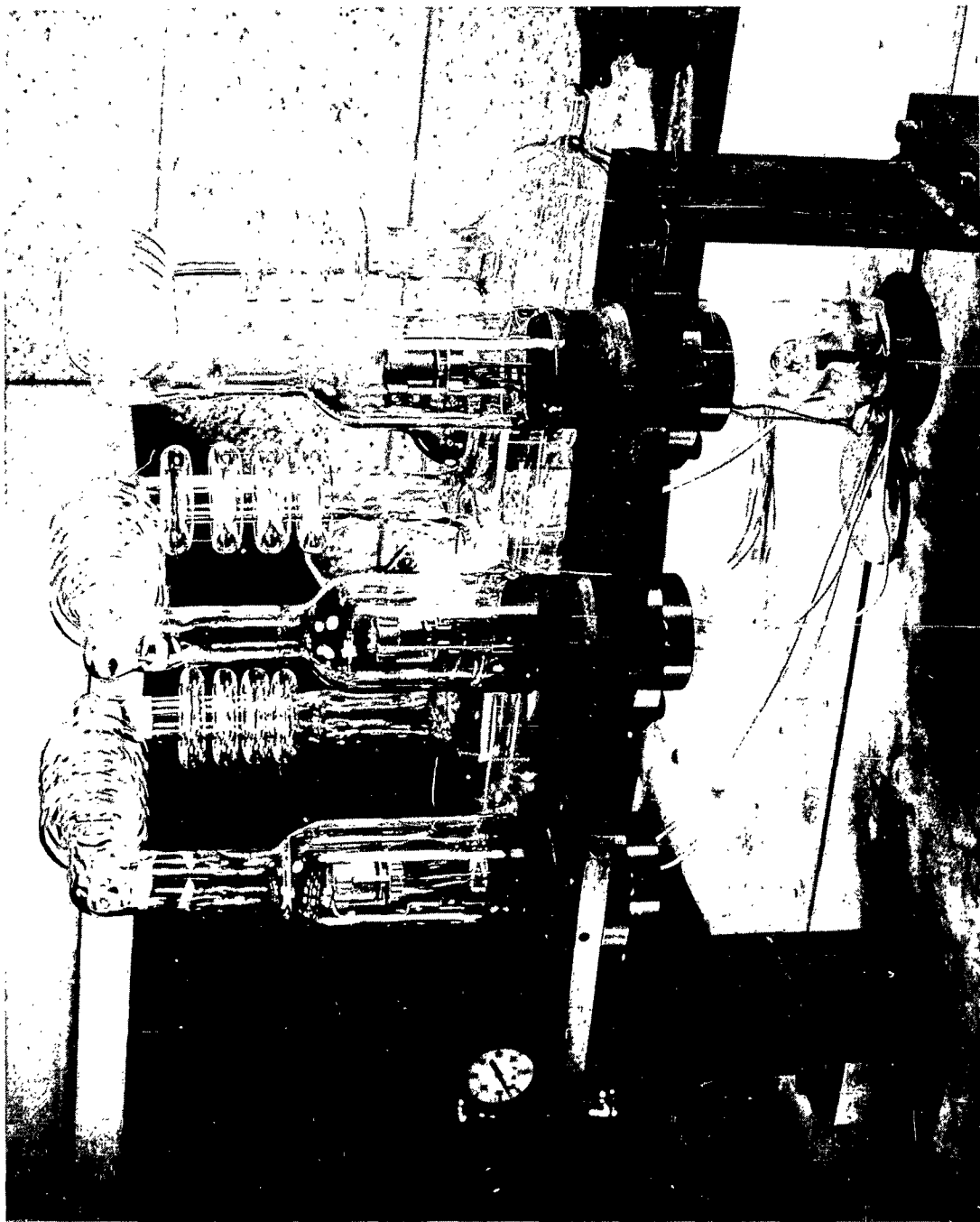


Figure 11 - Close up view of the three tubes containing the emitters and glass bellows.

The tube support stand which was fabricated from type 304 stainless steel incorporated two water cooled blocks at its base. This special design maintained the overall expansion rate of the stainless steel structure approximately equal to that of the glass manifold and associated connecting glass tubing to the three tubes. This prevented any glass breakage during the bakeout of the manifold and tubes. The bakeout was accomplished by a large oven (18 in. x 25 in. x 19 in.) which covered the full set of components shown in Fig. 11. This oven was capable of heating the high vacuum section to 450°C.

d. Portable Bakeout Oven and Power Supply

In order to outgas the vacuum manifold, it was necessary to bake out the entire system at 450°C. A very light portable oven was designed and fabricated in which a thin (0.016 in.) highly polished, chrome plated, stainless steel sheet was used as the heat barrier. Photographs of the oven and power supply are shown in Fig. 12, while the circuit diagram for the power supply is shown in Fig. 13.

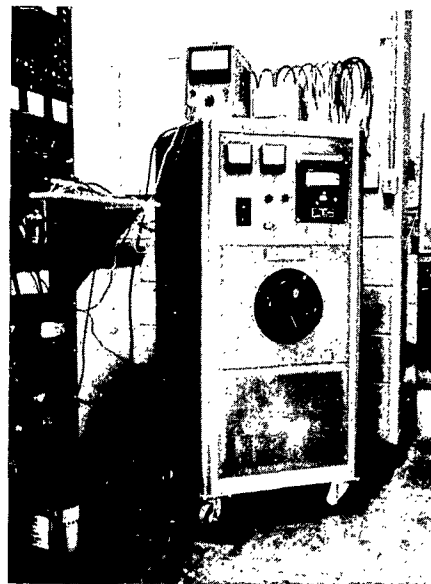
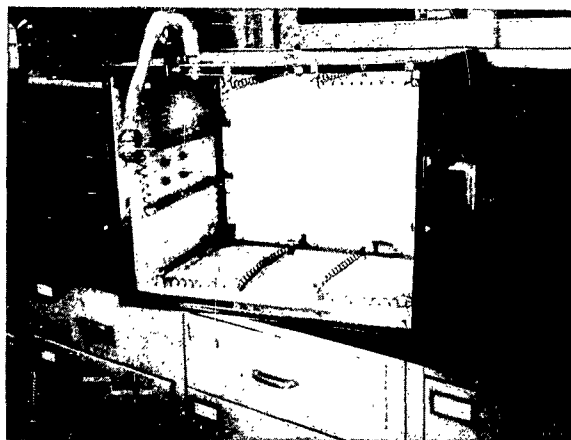
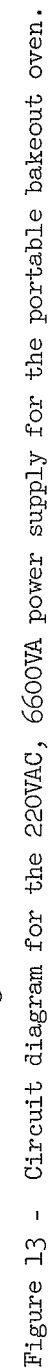


Figure 12 - Portable bakeout oven and power supply.





## 2. Tubes

In order to obtain comparative data, it was decided that tests made on three tubes processed under the same conditions would be the minimum number for reliable results. More than this number would complicate the testing and could offer but little additional information. The three tubes were mounted off the 2 in. diameter manifold along with two Bayard-Alpert ionization gauges--one gauge for spare. Corning No. 7052 glass was used as the envelopes for the three tubes. A pyrex to 7052 grade was used in the 1 in. diameter exhaust end of each tube.

The first requirement for the ultra high vacuum condition was satisfied by the system just described. The second requirement, that of being able to change emitters readily, was met by incorporating demountable tubes in the system, one of which is shown in Fig. 14. This photograph indicates the simplicity of the vacuum seal and other details. The component parts that make up the test section of the tube are shown in Fig. 15. The parts, reading from left to right are: collector, emitter guard ring, emitter, filament heater and emitter support. Because of the unique design of the demountable tubes, a detailed discussion of the various tube components are presented below.



Figure 14 - Tube components showing tube base, copper gasket and flange.

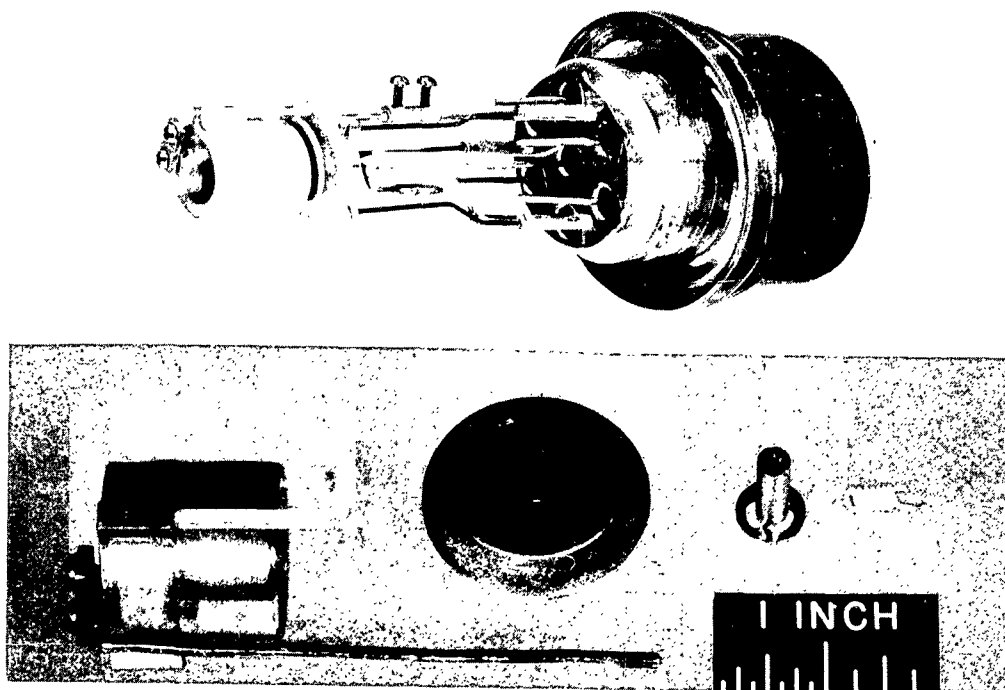


Figure 15 - Components ready for assembly into a tube stem.  
Left to right - collector, emitter shield, emitter  
and heater. Tube assembly above.

a. Emitter - Collector Arrangement

In order to expedite changing emitters, a special emitter holder was designed which consisted of two parts that screw together and clamp onto a thin perforated tantalum emitter support disc which had been previously spot welded to the emitter support sleeve. The emitter assembly was in turn supported from the tube base by three 0.040 in. diameter molybdenum wires. A detailed sketch of the emitter assembly is shown in Fig. 16.

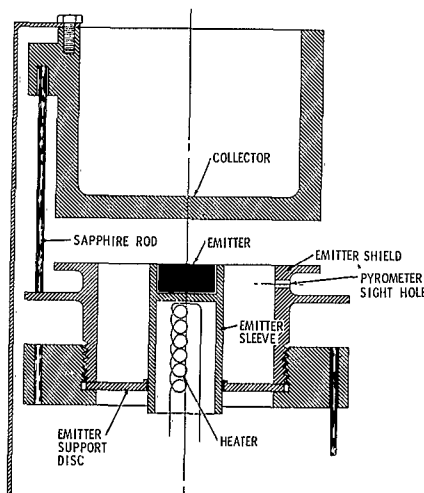


Figure 16 - Detailed sketch of emitter-collector arrangement.

A photograph of the emitter is shown in Fig. 17. The exact geometry and dimensions of the emitter and emitter support sleeve were shown in Fig. 11.

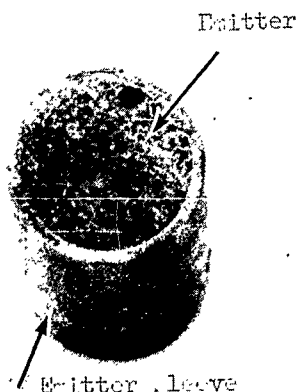


Figure 17 - Photograph of emitter with sleeve - 8X.

The collector was made from molybdenum, 1 in. in diameter by 1 in. long and relieved on the back side to reduce weight but still retain a large mass in order to provide a large thermal sink. This was important in order to minimize heating of the collector which in turn could produce gas pressure pulses in the tube. The collector was mounted from the emitter guard ring assembly by three sapphire rods and electrically connected by a 0.060 in. diameter wire to the tube base. The sapphire rods were 0.080 in. diameter and were used to maintain a 0.040 in. spacing between the emitter and collector.

b. Tube Base and Gasket Seal

Figure 18 shows a detailed sketch of the seal between the tube base and the vacuum system. A copper gasket 0.042 in. thick made the actual vacuum seal by being clamped between the two 2 in. Ultek<sup>(12)</sup> step flanges. The upper flange was held to the tube support stand by a set screw, while the lower flange was held to the stand by means of a ring and six stainless steel machine bolts. The bolts compressed the copper gasket between the two flanges by a shearing action of the step. This seal arrangement can withstand bakeout temperatures as high as 500°C. Seven ceramic feed throughs<sup>(14)</sup> were welded into the base. These feed throughs were used to make electrical connections to the heater, emitter, collector and thermocouples that were located on the various

tube parts. These feed throughs can withstand up to 15,000 volts. These were heliarc welded into the stainless steel base of the tube along with three 0.060 in. diameter nickel rods which were inserted into shallow holes in the base.

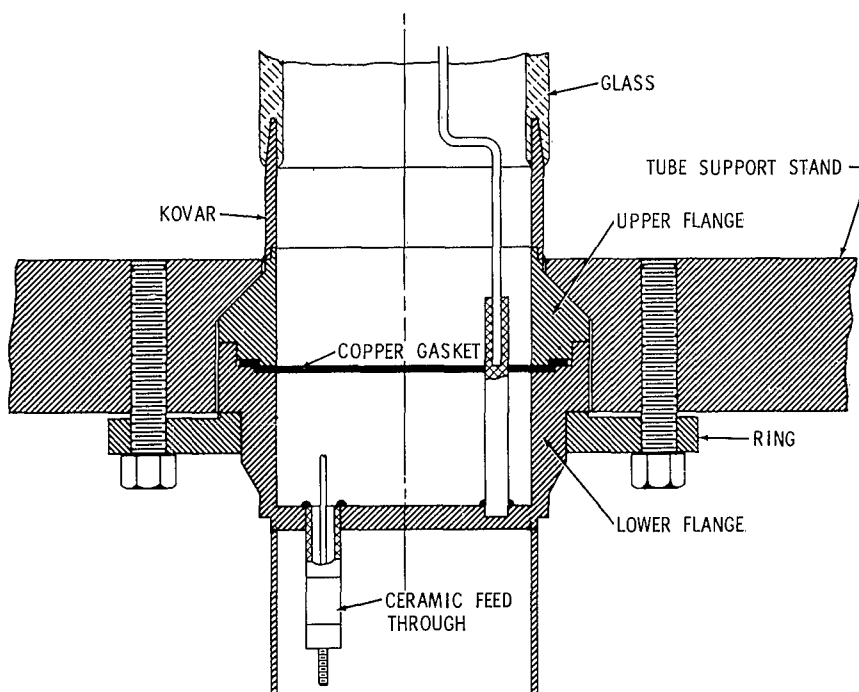


Figure 18 - Sketch of the copper gasket seal arrangement between the tube base and vacuum system.

### c. Heaters

A 1.2 ampere coated heater was used for heating the emitter to the desired temperature (900°C - 1400°C). The emitter power was approximately 14.5 watts for an emitter temperature of 1200°C. The heaters were purchased from the C and M Manufacturing Company, Bloomfield, New Jersey.

### 3. High Voltage Pulser

A high voltage pulser was designed and fabricated for obtaining the V-I characteristics from the various emitters. The design of the pulser was partially based on information received from the Naval Research Laboratories.<sup>(15)</sup> The characteristics of the pulser were:

Voltage:	0-15000 volt
Current:	10 amp (peak)
Pulse Width:	5-25μ sec
Rep. Rate:	30-120 pps

A schematic of the pulser and test diode is shown in Fig. 19. A simplified

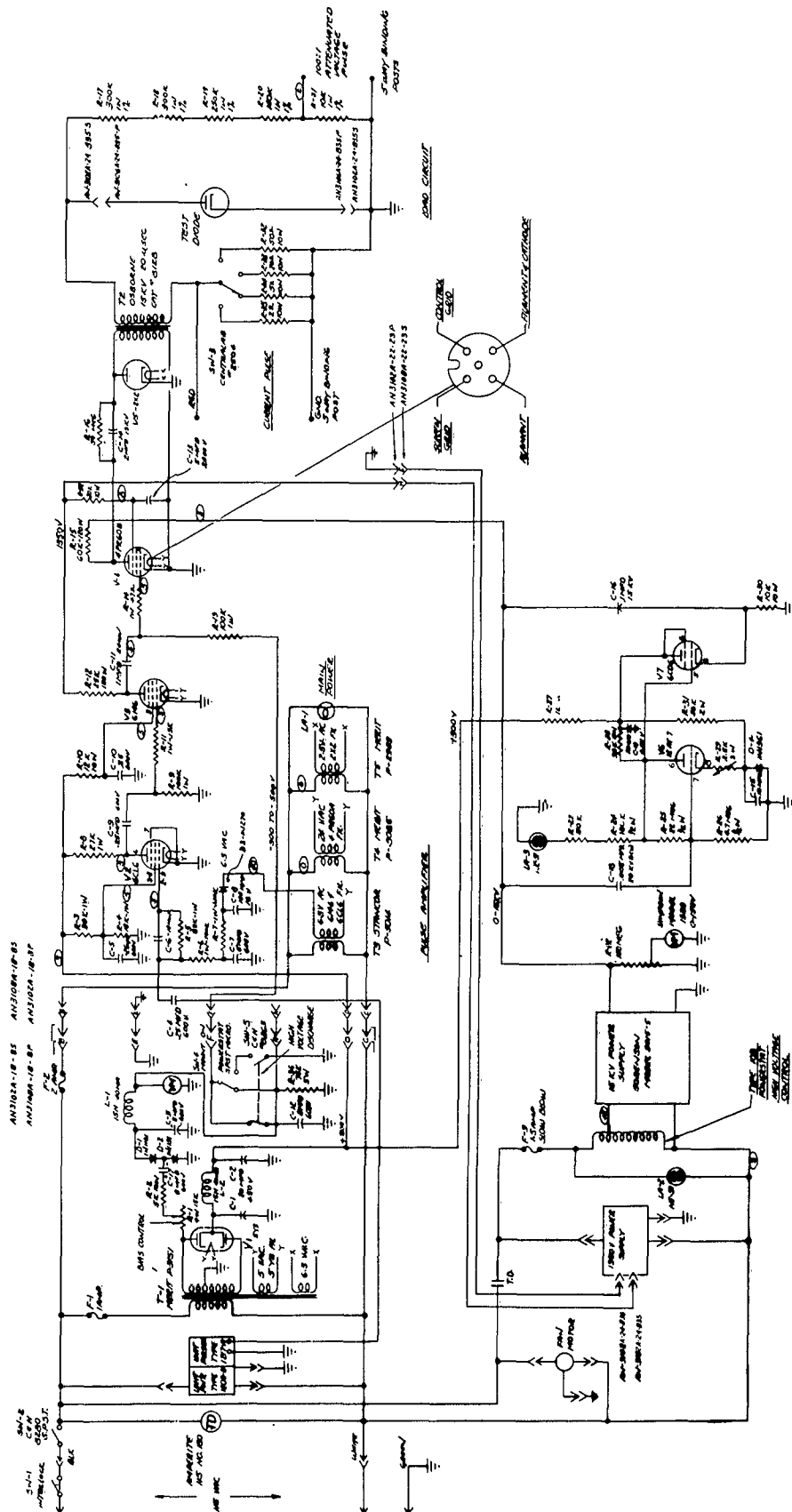


Figure 19 - High Voltage Pulsar.

block diagram of the measuring circuit is shown in Fig. 20. It may be noticed that a transformer has been added in Fig. 20. The original circuit was used where the diode under test could be operated with the collector electrically grounded and the emitter floating so that a negative pulse could be applied to the emitter.

A special 20  $\mu$ sec pulse width output transformer was designed<sup>(16)</sup> for this project to supply a positive pulse to the collector with the emitter grounded. Operating the emitter in this manner was an important feature as it simplified the heater circuit so it could function close to ground potential. This also allowed the base of the tubes to be more readily fabricated.

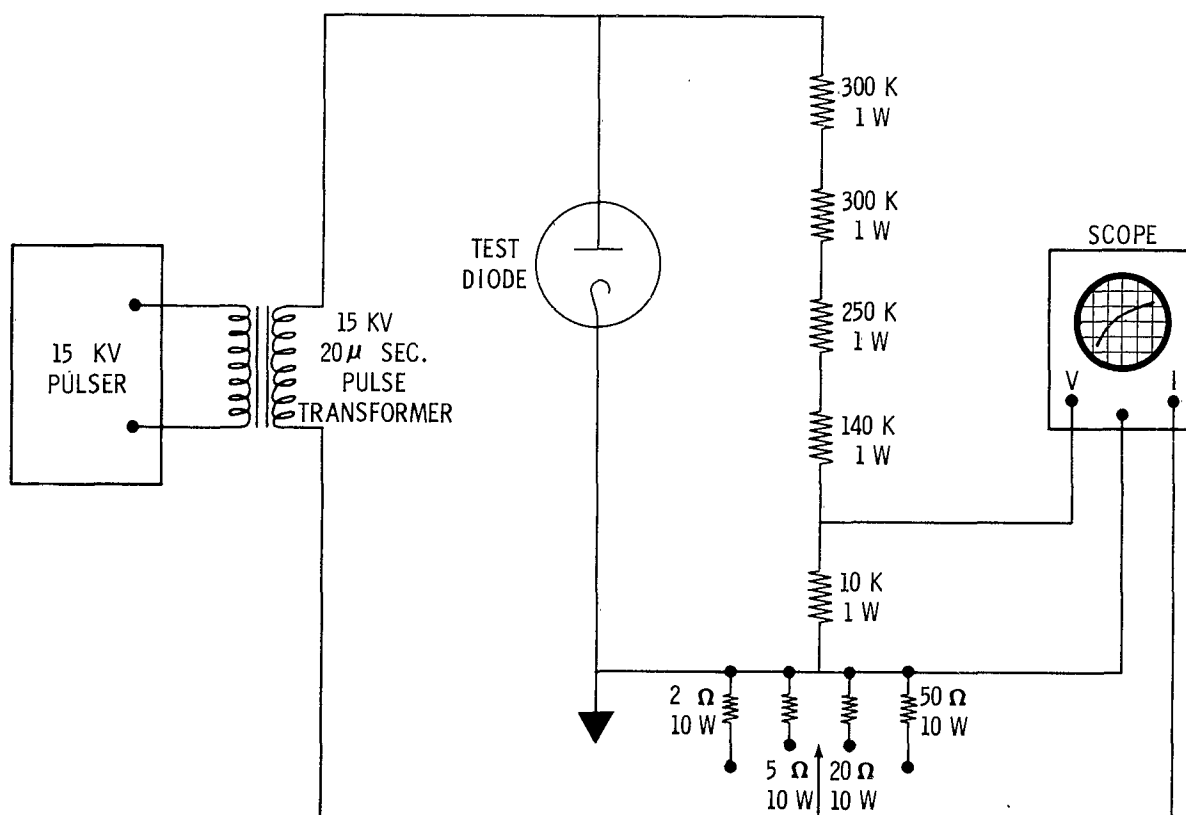


Figure 20 - Simplified circuit indicating how test diode is electrically connected.

## B. OPERATING PROCEDURE

### 1. Tube Processing

The fore and diffusion pumps were operated in the usual manner once the emitters were loaded onto the tube bases and the three bases inserted in the glass envelopes on the system. When the pressure reached the  $10^{-6}$  Torr scale, the ovens were placed on the system and the tubes were processed in the following manner:

- 1) The main oven is turned on and gradually brought up to a temperature of  $425^{\circ}\text{C}$ . The rate of temperature rise is determined by the pressure in the system which is maintained on the  $10^{-5}$  Torr scale. The system is baked at  $425^{\circ}\text{C}$  for 4 hours.
- 2) The trap oven is turned on and held to a temperature  $50^{\circ}\text{C}$  below that of the main oven for the same length of time.
- 3) After 4 hours bake and a pressure registering on the low side of the  $10^{-5}$  Torr scale the trap oven is removed.
- 4) When the trap is cooled sufficiently, liquid nitrogen is added.
- 5) The main oven is turned off and the tubes are allowed to cool gradually. The pressure should drop to  $10^{-7}$  Torr within 1/4 hour. At this time the emitters are heated to  $1000^{\circ}\text{C}$  for 5 minutes. The pressure is generally down on the  $10^{-9}$  Torr scale in three hours.
- 6) If for some reason the liquid nitrogen trap became empty, the system is rebaked for a couple of hours following the same procedure as mentioned above.

This procedure prevented sudden thermal shock to the glassware. A pressure of  $2 \times 10^{-9}$  Torr could be obtained.

To shut the system down, the liquid nitrogen was removed and the temperature of the trap allowed to rise. This resulted in a pressure of four to five orders of magnitude indicating that the trap was an effective pump. When the temperature of the trap was approximately room temperature the pumps were shut down in the usual fashion.

### 2. Emitter Processing

In order to obtain reliable and reproducible thermionic emission, standards were established in the processing of the tubes. Because these emitters were unique in their composition, the temperature range and the activation schedule had to be experimentally determined.

A norm was established for activating the emitters with the assurance that reliability could be expected from one type of emitter to another. This

schedule was experimentally determined on a number of sample emitters and has been so successful that V-I characteristics have been reproduced on active emitters over a period of days.

The norm for activating the emitters is as follows:

- A)
  - 1) Set temperature of emitters at 1250°C.
  - 2) Apply 250 to 300 volts dc.
  - 3) Monitor emission current on strip chart recorder.
  - 4) Age for 1.5 hours. The collector should glow at approximately 900°C which generally requires 100 ma emitter current. This current is maintained for approximately 1/2 hour.
  - 5) The emission current as recorded would become constant after about 1 hour with the pressure less than  $10^{-7}$  Torr.
- B)
  - 1) Following A - emitter temperature at 1250°C.
  - 2) Apply 7000 - 10,000 volts pulse.
  - 3) Monitor emission current on scope.
  - 4) Age for 1 hour or 0.5 hour after no change in current.
  - 5) Take V-I data going from high to low temperatures - and check at high temperature for reproducibility. The pulse width is approximately 20  $\mu$ sec and the repetition rate is 30 or 60 pulses per second (pps) depending on the best definition of the trace. The voltage is increased from 0 to 10,000 volts manually while the camera shutter is held open (approximately 5 sec.).
  - 6) If the data are not reproducible - pulse age and repeat step (5).

### 3. Emitter Temperature Calibration

As pointed out in an earlier section, the emitters were heated by tungsten heaters operating on ac. The temperature of the emitters was determined by an L and N optical pyrometer by viewing the side of the emitter sleeve through a sight hole located in the emitter shield. See Fig. 16. Reproducible calibrations as indicated in Fig. 21 show that the true temperature of the emitter surface agreed well with the temperature as measured by the optical pyrometer. The true temperature was measured for this calibration run by a chromel-alumel thermocouple. The range of temperature covered in conducting these experiments was from 800°C to 1350°C. Temperatures lower than 800°C were difficult to determine and also the electron emission was too minute to detect without more elaborate testing facilities. Higher temperatures than 1350°C generally were not attempted because of the limitation of the heaters. Figure 22 shows the voltage-current



characteristics of the heaters, and Fig. 23 shows the emitter temperature as a function of the heater input power.

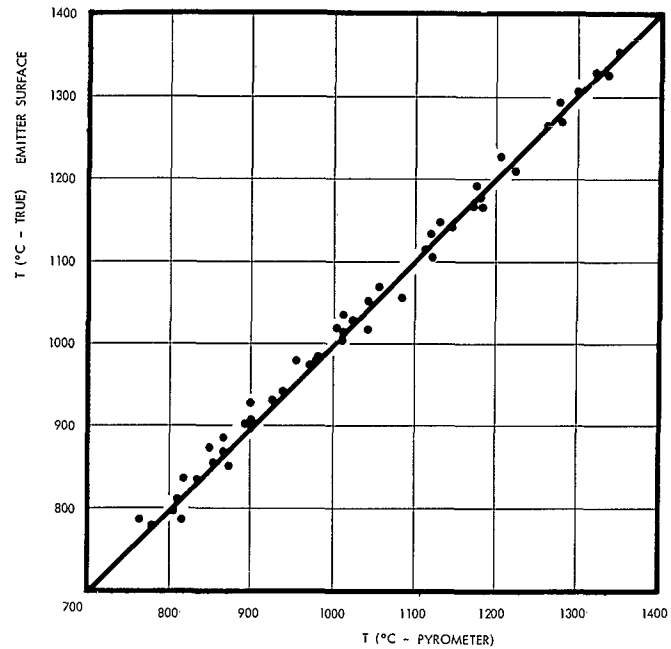


Figure 21 - Temperature calibration curve.

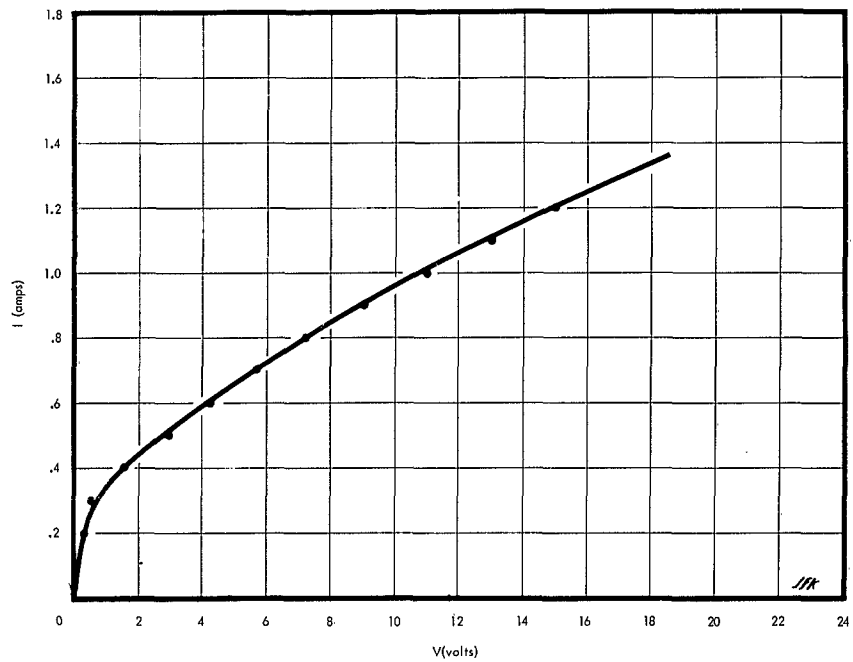


Figure 22 - Voltage-current relationship for heaters.

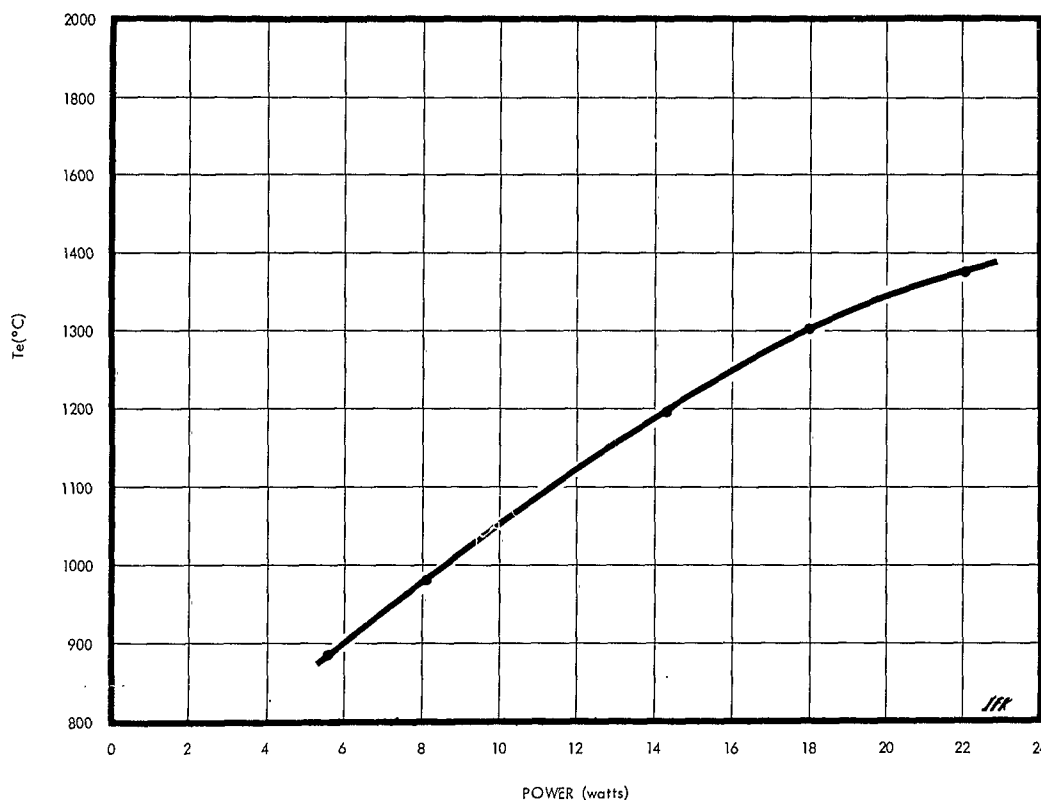


Figure 23 - Emitter temperature (true) vs heater power.

### C. THERMIONIC EMISSION

#### 1. Basic Equations

The thermionic emission characteristics of various materials are generally evaluated in terms of a work function and an emission constant. These values are obtained from the well known Richardson formula which defines the saturated emission current density,  $J_s$ , of an emitter as a function of its operating temperature, namely

$$J_s = A_o T^2 \exp \left( -\frac{e\phi}{kT} \right) \quad (7)$$

where  $J_s$  = saturated current density at zero electric field, amp/cm<sup>2</sup>  
 $e/k = 11,610^\circ\text{K}/\text{ev}$   
 $e$  = electron charge,  $1.6 \times 10^{-19}$  coulombs  
 $k$  = Boltzmann constant,  $1.38 \times 10^{-23}$  joules/ $^\circ\text{K}$   
 $T$  = temperature,  $^\circ\text{K}$   
 $\phi$  = work function, ev  
 $A_o$  = emission constant, amp/cm<sup>2</sup>- $^\circ\text{K}^2$  } material constants.

Experimentally the constants  $A_o$  and  $\phi$  in Eq. (7) can be determined from  $J_s$  and  $T$  for a given emitter material. A plot of  $\ln J_s/T^2$  versus  $1/T$ , known

as a Richardson plot, should be a straight line. The ordinate intercept determines  $A_0$  and the slope determines the work function  $\phi$ . Although the theoretical value of  $A_0$  is 120, experimentally it may range from  $10^{-7}$  to  $10^4$  amps/cm<sup>2</sup>-°K<sup>2</sup>. This is due, in part, to the dependence of the work function on the temperature.

This leaves  $J_s$  as the only unknown parameter to be experimentally determined. In Eq. 7,  $J_s$  is the saturated current density with zero electric field applied to the emitter, but this current cannot be measured directly. This saturated emission current density can be obtained indirectly, however, by applying a strong positive potential gradient to the emitter. Under these conditions the current from the emitter will increase even though the temperature is held constant and the emission is not affected by the space charge of the electrons. This implies that the work function is reduced when high fields are introduced. When a correction is made for the work function in the Richardson equation it is found that the emitter current density ( $J_e$ ) in the presence of the strong electric field is related to the saturation current density ( $J_s$ ) by

$$J_e = J_s \exp (4.40 \sqrt{E}/T) \quad (8)$$

where  $J_e$  is emission current density in amp/cm<sup>2</sup> in the presence of the strong electric field

$J_s$  is saturated emission current density in amp/cm<sup>2</sup> at zero field

$E$  is the field strength in volts/cm

$T$  is temperature (°K)

This expression is known as the Schottky equation. Experimentally this equation may be verified by plotting the logarithm of  $J_e$  against the square root of  $E$  where the electric field,  $E$ , is defined as the applied voltage,  $V$ , divided by the gap distance,  $d$ . The saturated current density,  $J_s$ , can now be determined by measuring  $J_e$  as a function of  $V$  for a given emitter while maintaining a constant emitter temperature and gap spacing. A plot of  $\ln J_e$  versus  $\sqrt{V}$ , known as a Schottky plot, should form a straight line in the Schottky region (high electric fields). The ordinate intercept, when extrapolating the straight line portion of this plot back to zero voltage, determines the saturated emission current density,  $J_s$ .

A Schottky plot of the experimental data results in a straight line whose slope is  $4.4 \sqrt{E}/T$  except at low values of potential where the current drops more rapidly than the simple Schottky equation predicts. Thus the standard practice is to extend the voltage sufficiently high to obtain a straight line through the experimental points at the high voltage end of the V-I plots. Generally, in the temperature range employed with the barium impregnated emitters, the slope exceeds the theoretical values.<sup>(17)</sup>

## 2. Experimental Data

The emitters, which were fabricated from the materials to be investigated, were incorporated into tubes and processed according to the steps listed in sections B-1 and B-2. During the emitter processing step, the emission current was recorded continuously on a strip chart recorder. A typical emitter activation curve is shown in Fig. 24. After the emission current had become stable, V-I characteristics of the emitter were obtained.

V-I characteristics were obtained for a series of at least 6 temperatures starting from the maximum temperature and working down. These data were recorded by a Polaroid camera with a setting at f/3 using 3000 speed/type 47 film. A typical photograph is shown in Fig. 25, where the abscissa represents the voltage (1000 v/cm) and the ordinate represents the current (100 ma/cm). These data were observed on a type 555 dual beam Tektronix oscilloscope. These photographs were taken as the pulse voltage was increased from zero to 10,000 volts (100,000 volts/cm) or until ionization occurred between the emitter and collector due to excessive current outgassing the collector or due to severe barium evaporation.

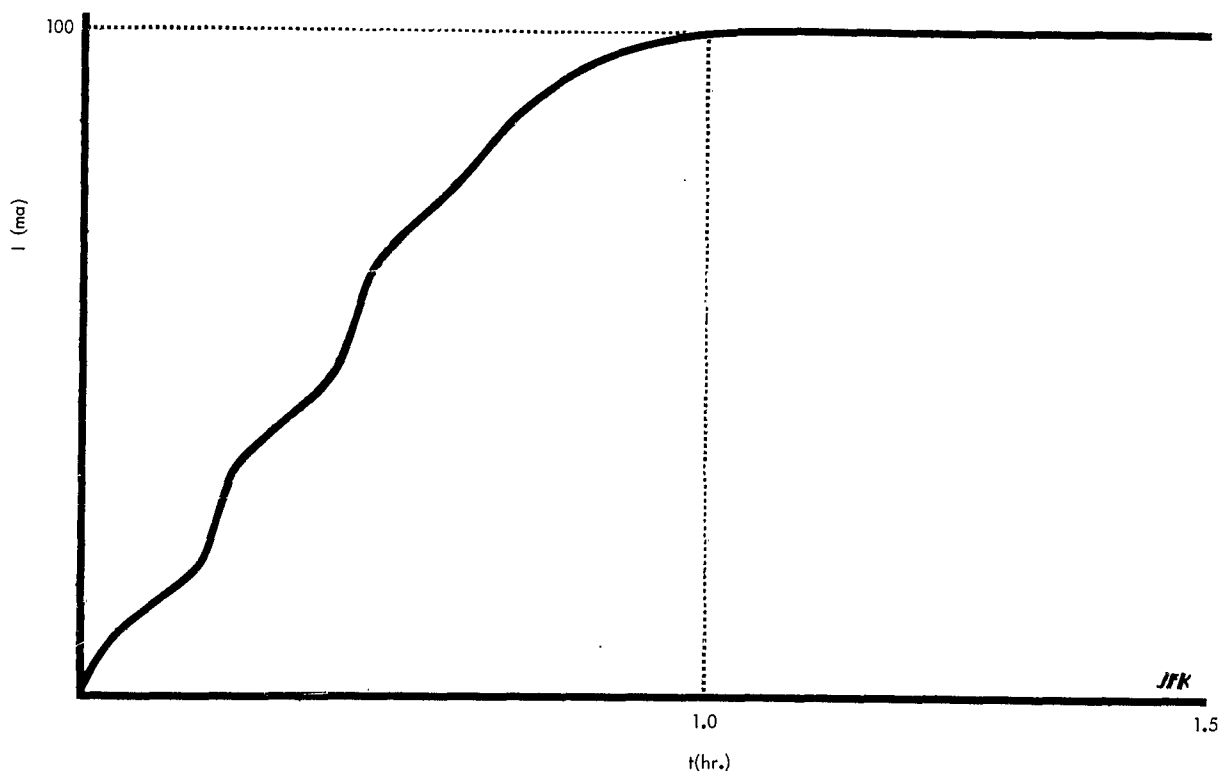


Figure 24 - Typical emitter activation curve.

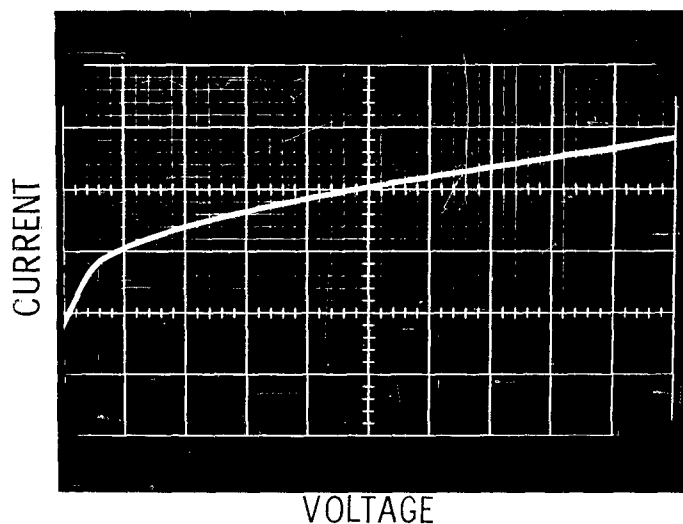


Figure 25 - Typical oscilloscope V-I trace.


The initial information was obtained from these photographs; each photograph representing the V-I characteristics from an emitter at one temperature. A value for the magnitude of the current was extracted from the photograph for at least 5 discrete voltage points starting from the high voltage end of the trace. (It was graphically found that a reasonably straight line could be constructed through at least five points before the Schottky line deviated from the data.) These points were from 9000 to 5000 volts in 1000 volt increments.

### 3. Data Evaluation

The procedure described above for evaluating the emission characteristics of the various emitters involves many long and laborious calculations. In order to facilitate these calculations, a computer code for use on the IBM 7090 was established. The input map for the code requires the current, voltage and temperature data obtained from the experiments along with the area of the emitter surface. An example of the input map is shown in Fig. 26. The units of the various quantities used in the input map are as follows:

- a = area -  $\text{cm}^2$
- V = voltage - volts
- T = temperature -  $^{\circ}\text{C}$
- I = current - ma

Figure 26



IBM 704 DATA SHEET

From this data the code is able to establish the saturated current density for the various temperatures and finally the work function and emission constant.

The slopes and intercepts for the various Schottky and Richardson curves are obtained by a least square fit of the input data. The equations used in this regression analysis are as follows:<sup>(18)</sup>

$$\text{slope} = m = \frac{\sum xy - n\bar{x}\bar{y}}{\sum x^2 - n\bar{x}^2} \quad (9)$$

$$y - \text{intercept} = y - mx \quad (10)$$

where

$$\begin{aligned} \sum xy &= x_1y_1 + x_2y_2 + x_3y_3 + \dots \\ \sum x^2 &= x_1^2 + x_2^2 + x_3^2 + \dots \\ n &= \text{number of data points} \\ \bar{x} &= \frac{1}{n} \sum x \\ \bar{y} &= \frac{1}{n} \sum y \end{aligned}$$

For the Schottky plot the x and y terms used in the regression analysis are as follows:

$$x = \sqrt{V} \quad (11)$$

$$y = \ln (I/a)$$

n = number of voltage points at each temperature

With this data the code calculates the slope and y- intercept of the Schottky curve for each temperature. The saturated current density is then obtained by taking the antilog of the y- intercept, namely

$$J_s = \exp (\bar{y} - m\bar{x}) \quad (12)$$

After the saturated current density has been established for each temperature, the Richardson curve is obtained. Again with the use of Eqs. 9 and 10 where

$$x = 10,000/T \quad (13)$$

$$y = \ln (J_s/T^2)$$

n = number of temperature points

the slope and y- intercept of the Richardson curve are calculated. The y- intercept defines the emission constant  $A_0$  used in Eq. 7 namely

$$A_0 = \exp (\bar{y} - m\bar{x}) \quad (14)$$

The slope is used to obtain the work function in the following manner. First, Eq. 7 is newly written in the following form:

$$\ln \frac{J_s}{T^2} = \ln A_o - 1.16 \phi \frac{10,000}{T} \quad (15)$$

Since the Richardson curve as calculated by the code is based on a plot of  $\ln(J_s/T^2)$  vs  $10,000/T$ , the slope of the Richardson line is  $m = -1.16 \phi$ . The work function is then obtained by dividing the slope of the line by  $-1.16$  namely

$$\phi = m/-1.16. \quad (16)$$

In many correlations it is desirable to compare the work function of various emitters when the emission constant is set equal to the theoretical value of  $120 \text{ amps/cm}^2 \cdot \text{K}^2$ . This work function which is defined as the effective work function, can be derived from Eq. 15. Inserting  $A_o = 120 \text{ amp/cm}^2 \cdot \text{K}^2$  into Eq. 15

$$\ln \frac{J_s}{T^2} = \ln 120 - 1.16 \phi \frac{10,000}{T} \quad (17)$$

Equating Eqs. 15 and 17

$$(\phi_{\text{eff}} - \phi) \frac{1.16 \times 10^4}{T} = \ln \frac{120}{A_o}$$

then

$$\phi_{\text{eff}} = \phi + \left[ 8.62 \times 10^{-5} \ln \frac{120}{A_o} \right] T$$

or

$$\phi_{\text{eff}} = \phi + \alpha T \quad (18)$$

where  $\alpha$  is the work function temperature coefficient and is given as

$$\alpha = 8.62 \times 10^{-5} \ln (120/A_o) \quad (19)$$

Figure 27 shows the code calculations based on the input data presented in Fig. 26. The upper portion of the computer sheet lists the input data, namely emitter area, number of temperature points, number of voltage points and a table showing the emission current as a function of voltage and temperature. This information is printed out at this point so that a check can be made on the actual data that was supplied to the IBM 7090.



FIGURE 27  
WORK FUNCTION CALCULATIONS

URANIUM-BARIUM-RHENIUM EMITTER 7525R PULSED RUN

INPUT

AREA 0.0707 NO. OF TEMPERATURES 6 NO. OF VOLTAGES 5

VOLTAGES

TEMP 9000. 6000. 7000. 6000. 5000.

1025.	22.00	20.00	19.00	18.50	18.00
1063.	37.50	35.00	33.60	31.20	30.00
1133.	80.00	76.00	72.00	67.00	64.00
1170.	112.00	104.00	98.00	94.00	88.00
1195.	125.00	117.00	110.00	103.00	98.00
1245.	162.00	155.00	145.00	137.00	130.00

OUTPUT

VOLTAGE	SQ RT VOLTAGE	SCHOTTKY DATA				
		1025.	1063.	1133.	1170.	1195.
9000.	0.	1.4E-01	2.2E-01	4.6E-01	6.3E-01	6.7E-01
8000.	94.87	3.1E-01	5.3E-01	1.1E 00	1.6E 00	1.8E 00
7000.	89.44	2.8E-01	5.0E-01	1.1E 00	1.5E 00	1.7E 00
6000.	83.67	2.7E-01	4.8E-01	1.0E 00	1.4E 00	1.6E 00
5000.	77.46	2.6E-01	4.4E-01	9.5E-01	1.3E 00	1.5E 00
	70.71	2.5E-01	4.2E-01	9.1E-01	1.2E 00	1.4E 00
SLOPE		0.008	0.009	0.009	0.010	0.009

J(S) (FITTED)  
1.5202E-01  
2.2043E-01  
4.1631E-01  
5.6939E-01  
6.9781E-01  
1.0289E 00

RICHARDSON DATA  
J(S)/T\*\*2 (FITTED)  
9.0E-08  
1.2E-07  
2.1E-07  
2.7E-07  
3.2E-07  
4.5E-07

TEMP 10000/T  
1025. 7.70  
1063. 7.49  
1133. 7.11  
1170. 6.93  
1195. 6.81  
1245. 6.59

SLOPE = -1.4322

INTERCEPT = 5.6E-03

WORK FUNCTION = 1.235

TEMPERATURE COEFFICIENT = 0.860E-03

FOR T = 1100 DEG C PHI EFFECTIVE = 0.242E 01

Section 1

Section 2

Section 3

The output section of the code shown in Fig. 27 is divided into three sections. The first section lists the Schottky data. Figure 28 shows the Schottky curves for the values given in this Schottky section. It may be noticed that in general, the straight line deviates from the experimental points for voltages less than the discrete top five. The  $J$  intercept is determined by extrapolating a straight line from the least square fit of the five points. This intercept gives the  $J_s$  value.

The second section in Fig. 27 shows the Richardson data when using the  $J_s$  values from the Schottky curves. Figure 29 shows the Richardson plot as obtained from these data. The straight line can be drawn from the values given in the column  $J(S)/T^{*2}$  (Fitted) which is a result from the least square fit. The last column  $J(S)$  (Fitted) is that saturated current density computed when using the least square fit values for the Richardson curve. It may be noticed that they agree reasonably well with the actual  $J_s$  values in the second section.

The third section in Fig. 27 shows the final results, i.e. the intercept ( $A_o = 5.6 \times 10^{-3}$ ); the work function ( $\phi = 1.235$ ); the temperature coefficient ( $\alpha = 0.860 \times 10^{-3}$ ) and ( $\phi_{\text{effective}}$  at  $1100^\circ\text{C} = 0.242 \times 10^1$ ).

The data compiled from the emitters are summarized in Table 12. The left side indicates the chemical composition of the emitters, while the right side shows the emission characteristics, listing  $A_o$ ;  $\alpha$  and  $\phi_{\text{eff}}$  at  $1100^\circ\text{C}$  for comparative purposes. It should be emphasized that for each of these emitter types there were three emitter samples tested. And in many instances some samples were tested more than once for obtaining additional data or for supplemental data such as temperature calibrations, voltage breakdown characteristics, etc.

The data shown under emission characteristics represent, in most instances, a mean average for the three samples of each type of emitter. In a few cases data from one sample from one emitter type varied from the other two samples and was not considered in representing that type of emitter. It was for this very reason that three samples (instead of one) were tested, in order to obtain reliable data. Generally, when these discrepancies occurred, it could be traced to temperature gradients between the shell and the emitter surface, to emitters that activated relatively abnormal, etc.

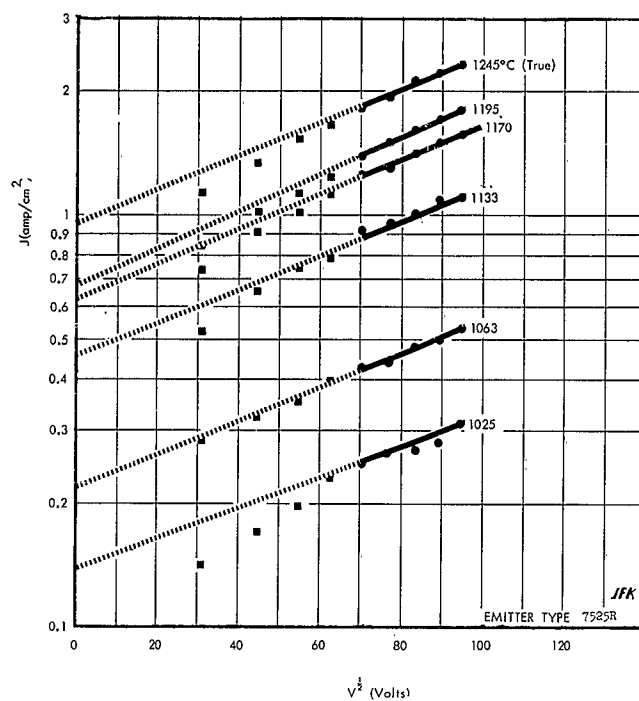


Figure 28 - Schottky Curves

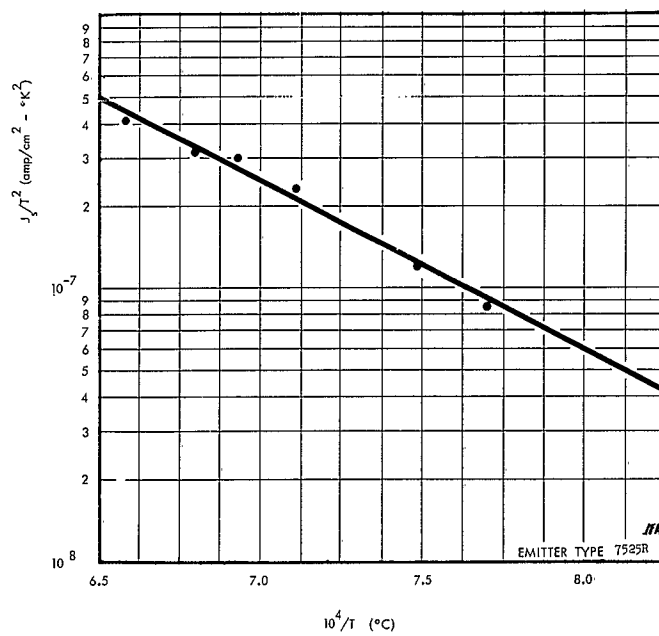


Figure 29 - Richardson Curve

TABLE 12

Emitter Type	Chemical Composition				Emission Characteristics					
	BaO Content w/o	V/O Oxide	M/O BaO	M/O UO <sub>2</sub>	V/O Metal	$A$ (a./cm <sup>2</sup> -°K <sup>2</sup> )	$\phi$ (ev)	$\alpha$ x 10 <sup>-4</sup> (ev/°K)	$\phi$ <sup>eff</sup> at 1100°C (ev)	Number of Tests
7575	33	75	75	25	25 W	2.3	1.62	3.4	2.08	4
2575	7	25	75	25	75 W	3.5 x 10 <sup>-7</sup>	0.16	16.9	2.49	6
7525	9	75	25	75	25 W	1.9 x 10 <sup>-2</sup>	1.46	7.56	2.50	3
2525	2	25	25	75	75 W	3.0 x 10 <sup>-6</sup>	0.49	15.1	2.56	4
7545	18	75	45	55	25 W	8.2 x 10 <sup>-2</sup>	1.43	6.29	2.30	4
7560	25	75	60	40	25 W	3.3	1.76	3.11	2.19	4
7570	30	75	70	30	25 W	2.5	1.61	3.32	2.07	4
2560	5	25	60	40	75 W	3.6 x 10 <sup>-4</sup>	1.09	11.0	2.59	4
7545*	18	75	45	55	25 W	5.7 x 10 <sup>-1</sup>	1.95	2.86	2.34	3
7560*	25	75	60	40	25 W	2.1 x 10 <sup>-1</sup>	1.44	5.49	2.20	4
7570*	30	75	70	30	25 W	8.89	1.67	2.88	2.07	3
2560*	5	25	60	40	75 W	Not tested				
7575 R	31	75	75	25	25 Re	5.6	1.73	2.66	2.09	8
2575 R	6	25	75	25	75 Re	8.7 x 10 <sup>-1</sup>	1.76	4.25	2.35	7
7525 R	9	75	25	75	25 Re	4.7 x 10 <sup>-3</sup>	1.21	8.77	2.42	5
2525 R	2	25	25	75	25 Re	6.6 x 10 <sup>-6</sup>	0.19	16.90	2.51	3

\* The starred specimens were fabricated with the oxide mixture reduced to minus 325 mesh. All other samples were fabricated with the oxide reduced to minus 100 mesh.

Graphs of the information that is tabulated in Table 12 are presented in the following figures. Figures 30 and 31 show the effective work function plotted against temperature for tungsten and rhenium respectively. These essentially, show how  $\alpha$  varies between emitter types. The curves shown in Fig. 30 are for the 100 mesh oxide samples. The curve representing the dispenser cathode is that reported in reference 20. It may be noticed that the 7570 and 7575 type emitters are comparable to the dispenser type.

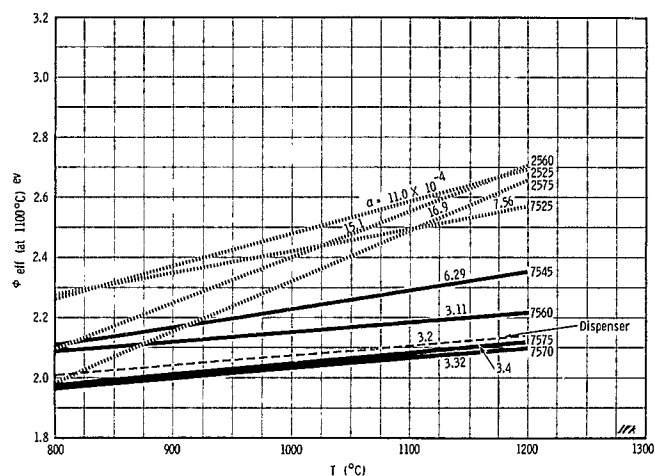


Figure 30 - Family of work function dependence on temperature curves for BaO-UO<sub>2</sub>-W emitters.

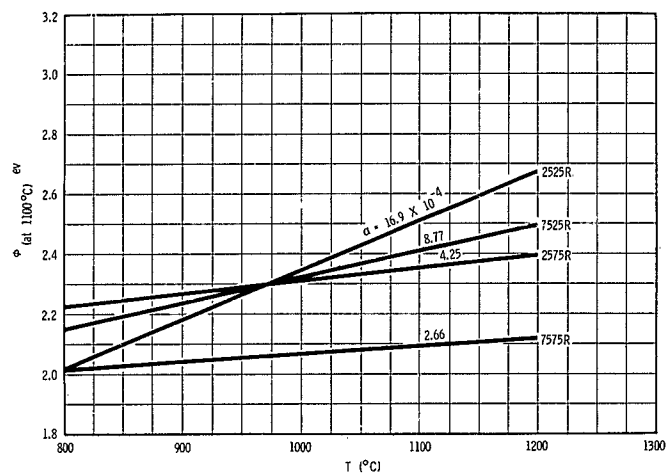


Figure 31 - Family of work function dependence on temperature curves for BaO-UO<sub>2</sub>-Re emitters.

Figure 32 shows how the BaO content affects the effective work function. The BaO content is shown in Table 12 for each of the emitter types. There appears to be a linear relation between the BaO content and the effective work function as may be noticed, with the 7570 and 7575 type samples giving the lowest work function.

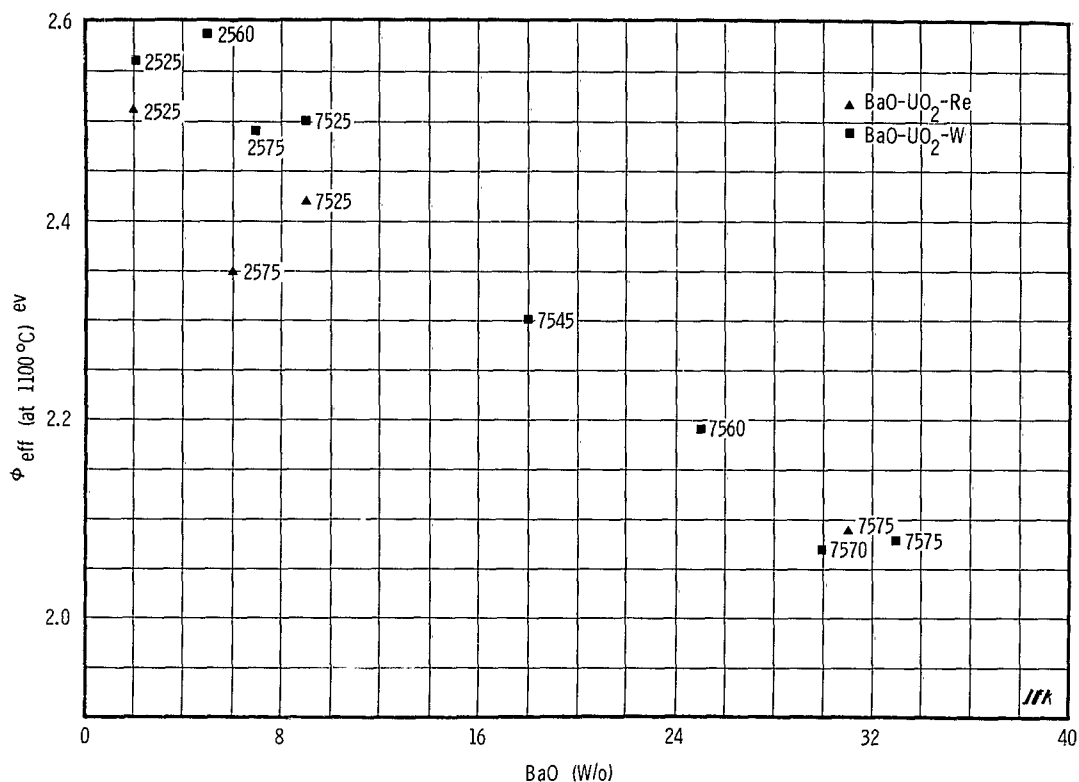


Figure 32 - Effect of barium oxide content on work function for BaO-UO<sub>2</sub>-W and Re emitters.

Figures 33 and 34 show the saturation current densities vs temperature for tungsten and rhenium respectively. It may be observed that the curves follow the same relative order as does the BaO content. A current density of 10 amps/cm<sup>2</sup> at 1175°C was recorded for the 7570 type as shown in Fig. 33. Currents of this order were observed for the 7575 type but excessive ionization due to barium evaporation occurred when operating this type of emitter above 1100°C. This factor also limited the temperature for the 7570 type to approximately 1200°C. As a reference, the current densities reported for the 7570 type are at least comparable to those reported for the dispenser cathode.

The curves found in the lower right hand side of Fig. 33 are those representing emitters which have a relatively low BaO content. It may be noticed that not only are the current densities low but that the slopes of the curves are widely spread. This is due in part to the fact that these particular types of emitters were exceedingly hard

to activate and were very sensitive (emission wise) to any gas bursts. The end result was that they were unstable and it was very difficult to obtain good reliable emission data.

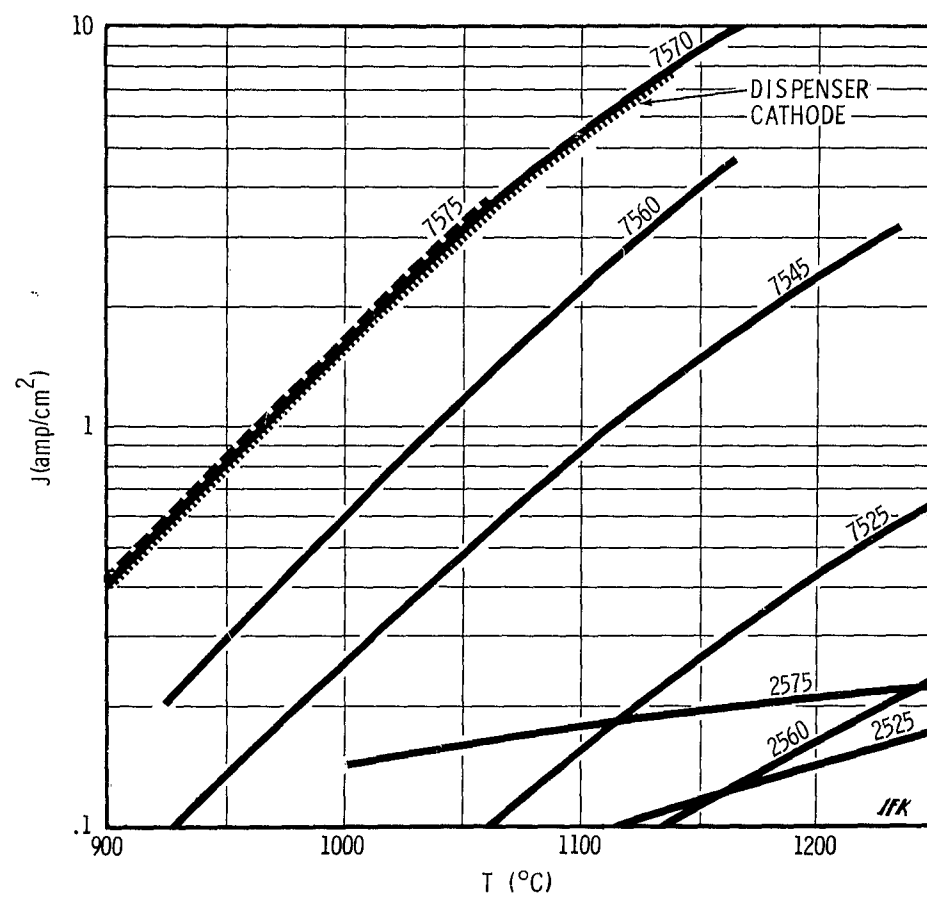


Figure 33 - Saturation current density for BaO-UO<sub>2</sub>-W emitters.

It may be noticed that the curves in Fig. 34 for rhenium follow the same general pattern as that for tungsten and therefore further investigation with rhenium was not deemed advisable at the expense of the tungsten series.

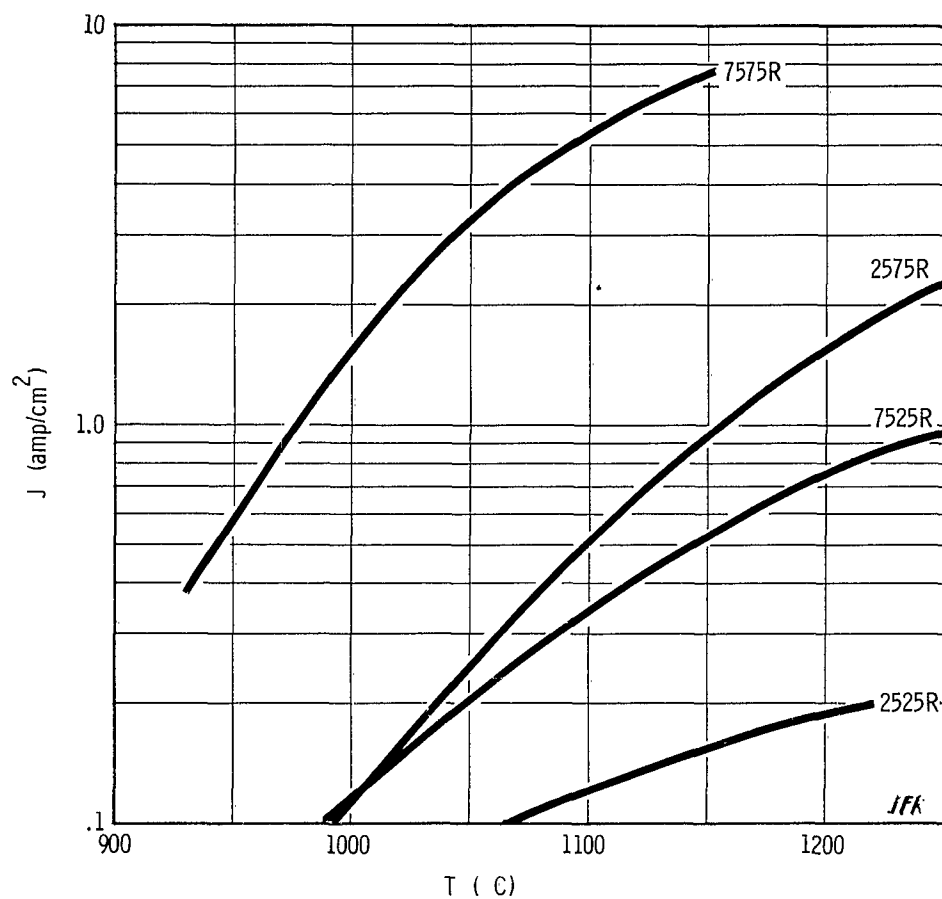


Figure 34 - Saturation current density for BaO-UO<sub>2</sub>-Re emitters.



One of the properties that could affect the electron emission is the size of the particles that are used in the emitter. For this reason a number of emitters were made which had the oxide reduced to 325 mesh rather than 100 mesh. The 325 mesh types are marked with an asterisk in Table 12.

It was found from thermionic emission data studies that the oxide particle size (within the range 100-325) had very little effect on the electron emission as can be seen by comparing the effective work function of the 325 mesh type with the 100 mesh type. One overall comment on the 325 mesh emitters is that they were much more difficult to activate prior to obtaining emission data. One reason for this may be that the density is greater in the 325 mesh than that for the 100 mesh and therefore more difficulty may be encountered for the barium to diffuse through the grain boundaries on its way to the surface of the emitter. Once the emitters have been activated the emission characteristics appear to be independent of oxide particle size within the limits of this experiment.

#### IV. EMISSION MICROSCOPE STUDIES

In recent times the practical utilization of impregnated emitters commands a great deal of interest, especially in cases where it is necessary to obtain comparatively large electron emission densities at moderate temperatures. Such emitters schematically consist of porous matrices containing an appropriate activating agent, usually BaO. Under actual operating conditions the barium oxide is reduced to free barium atoms. These free barium atoms, diffusing through the porous matrix onto the external surface, cover the emitter surface to produce the desired emission characteristics. The electrons are then released from the tungsten whose work function has been lowered by the absorption of a monatomic layer of barium. In order to gain an insight into this mechanism of barium transfer, various barium containing emitters were tested on the thermionic emission microscope.

##### A. Barium Oxide - Uranium Oxide Emitters

The most direct method of showing whether the tungsten surface is completely or partially covered with barium is by means of the emission microscope. Thus we have employed this method on several of the BaO-UO<sub>2</sub>-W emitter samples. The composition and effective work function of the various emitters that were tested on the microscope are listed in Table 13.

Table 13

Sample No.	Characteristics of BaO-UO <sub>2</sub> -W Emitters	
	Chemical Composition	Effective Work Function at 1100°C, ev
7575	75 v/o (75 m/o BaO-25 m/o UO <sub>2</sub> )-25 v/o W	2.08
2575	25 v/o (75 m/o BaO-25 m/o UO <sub>2</sub> )-75 v/o W	2.49
7525	75 v/o (25 m/o BaO-75 m/o UO <sub>2</sub> )-25 v/o W	2.50
2522	25 v/o (25 m/o BaO-75 m/o UO <sub>2</sub> )-75 v/o W	2.56

The effective work function of these various emitters were obtained from Table 12.

Photographs of the emission patterns obtained from the various samples are shown in Fig. 35. The emission pattern in each case was obtained from the free barium that was released by a reaction between the barium oxide and tungsten. From the first set of photographs at 980°C it can be noted that the free barium was mainly confined to the boundaries between the BaO-UO<sub>2</sub> particles and tungsten matrix. At this temperature the free barium did not have sufficient time to diffuse over the surface of the tungsten which remained dark in the photographs. The effect of barium oxide concentration in the various emitters can also be noted. As the temperature of the emitters was increased to 1095°C, it can be noted in the second row of photographs that the free barium was beginning to diffuse across the tungsten surface.

The various emitters were then heated to 1230°C and held at this temperature for two minutes in order to increase the free barium content of the samples. This process is usually called 'activation'. The samples were then cooled to 1070°C for viewing. The resulting surface structures are shown in the third row on Fig. 35. This set of photographs indicates that the activation step increased the overall electron emission slightly.

From the photographs listed in Fig. 35 only qualitative data on the emission characteristics of the various emitters can be obtained. Such information as the degree of barium coverage, and the effect of temperature, time and barium concentration on the emission pattern can be noted. Quantitative data such as work function and emission constant cannot be evaluated from the photographs.

#### B. Philips Cathode Emitter

The characteristics of electron emitting surfaces are interesting from the standpoint of obtaining information on the mechanisms involved in the emission process. This is particularly true of emitters that contain their own supply of activator, such as barium. This type of emitter must supply free barium to the surface of the emitter at a controlled rate in order to maintain the desired work function. In an attempt to gain some insight into the emission process, the surface characteristics of a Philips impregnated-type B cathode emitter were investigated on the

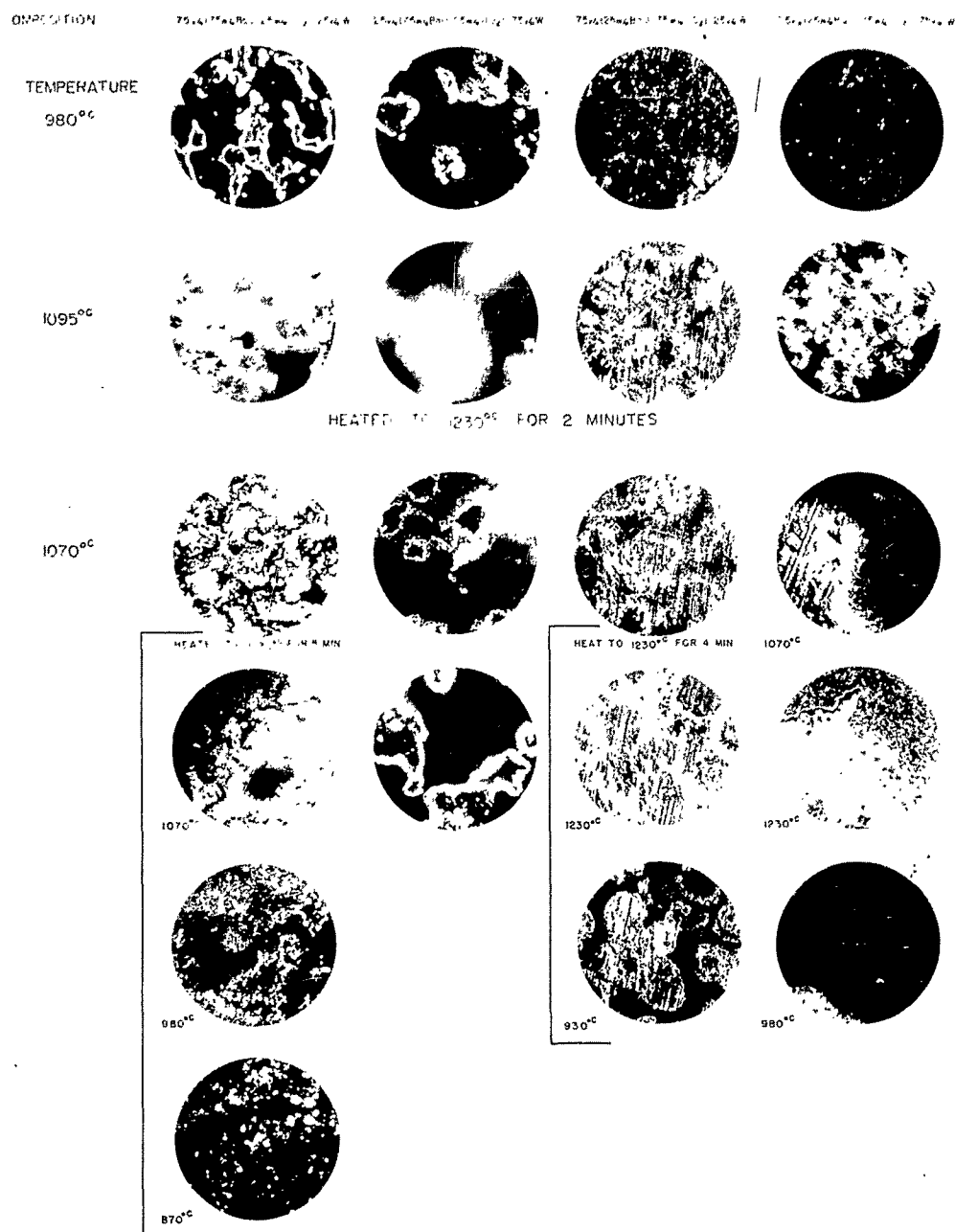


Figure 35 - Emission patterns of various BaO-UO<sub>2</sub>-W emitters.

thermionic emission microscope. The results that were obtained from this preliminary investigation were published in the Journal of Applied Physics.<sup>(17)</sup> The results indicated that after the Philips cathode emitter had been adequately activated, the surface structure was a function of its operating temperature. For example, at 1040°C the surface of the emitter showed a granular structure. This granular structure was reminiscent of the grain structure observed in polycrystalline metal specimens and was undoubtedly, the grain structure of the underlying porous tungsten body. As the temperature was increased to 1090°C, the granular structure disappeared and a monotone surface of medium intensity was seen. Finally, as the temperature was increased to 1150°C, the granular structure reappeared and persisted up to the upper temperature limit of the microscope.

The thermionic emission properties of the underlying metal make themselves evident in the emission pattern when the barium is present only in a very thin layer usually defined as a monolayer. This absorbed layer of barium produces an outwardly directed positive dipole moment which results in a sizable reduction in work function of the base material. If the barium layer becomes thicker than the required monolayer, the work function will be increased and the structure of the underlying base material may disappear.

On the basis of the above discussion, a qualitative explanation for the various surface appearances of the Philips cathode emitter can be established. Basically the thickness of the barium layer and thus the emission pattern depends upon a delicate balance between the production, diffusion and evaporation of barium in the emitter. Initially the barium is confined within the voids of the tungsten matrix in the form of tribarium aluminate. As the temperature of the emitter is increased, the tribarium aluminate slowly reacts with the tungsten matrix to produce a specific concentration of free barium within the emitter. This free barium will then diffuse from the core of the emitter to its surface where it will spread across the emitting surface. At the same time that barium is being produced and diffused to the surface, it is also being evaporated from the surface. The thickness of the barium layer that develops on the surface of the emitter then will be governed by rate of these three processes.

A graphical representation of the three processes as a function of temperature is shown in Fig. 36.

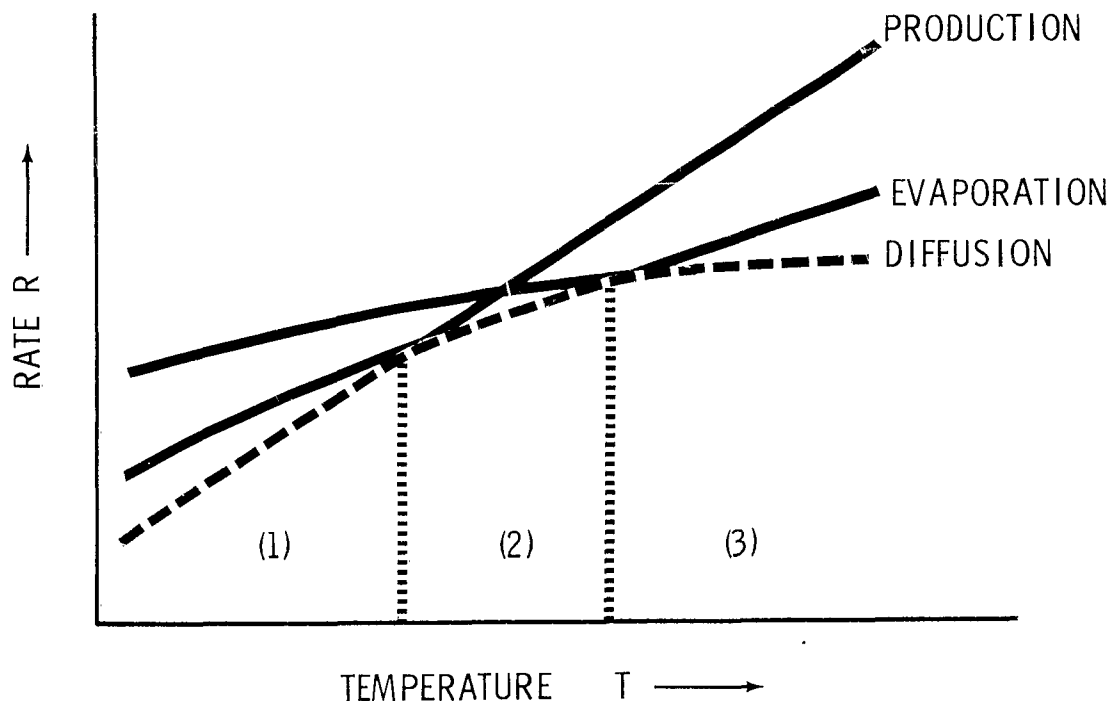


Figure 36 - Barium processes that are taking place in a Philips cathode emitter.

For example, at low temperatures (region 1) the production of free barium due to the reaction between the barium compound and the tungsten matrix is lower than the diffusion and evaporation rates. Thus only a thin film of barium can exist on the surface of the emitter. In like manner, at high temperatures (region 3) the evaporation rate exceeds the ability for free barium to diffuse to the surface, again resulting in a minimum barium thickness. At some intermediate temperature range, on the other hand, the evaporation rate of barium from the surface of the emitter becomes controlling. Under these conditions the evaporation rate is lower than the production and diffusion rates, and thus an excessive barium layer is developed on the surface of the emitter. This results in the monotone characteristics of the emitter as observed with the electron microscope.

The temperature range for the various regions will change with the operating life of the emitter. For example during the initial part of life, the free barium that reaches the emitter surface is produced very close to the surface. As the

life of the emitter is extended, the free barium must migrate from deeper sections within the core. This change in migration depth will have an effect of the overall diffusion process which in turn will govern the temperature at which the various processes become controlling.

### C. Emission Current

In order to attempt a correlation between the surface structure of the emitter and the emission current from the emitter, a collector was inserted into the electron path of the microscope. Figure 37 shows a schematic of the thermionic emission microscope with the collector inserted in the system.

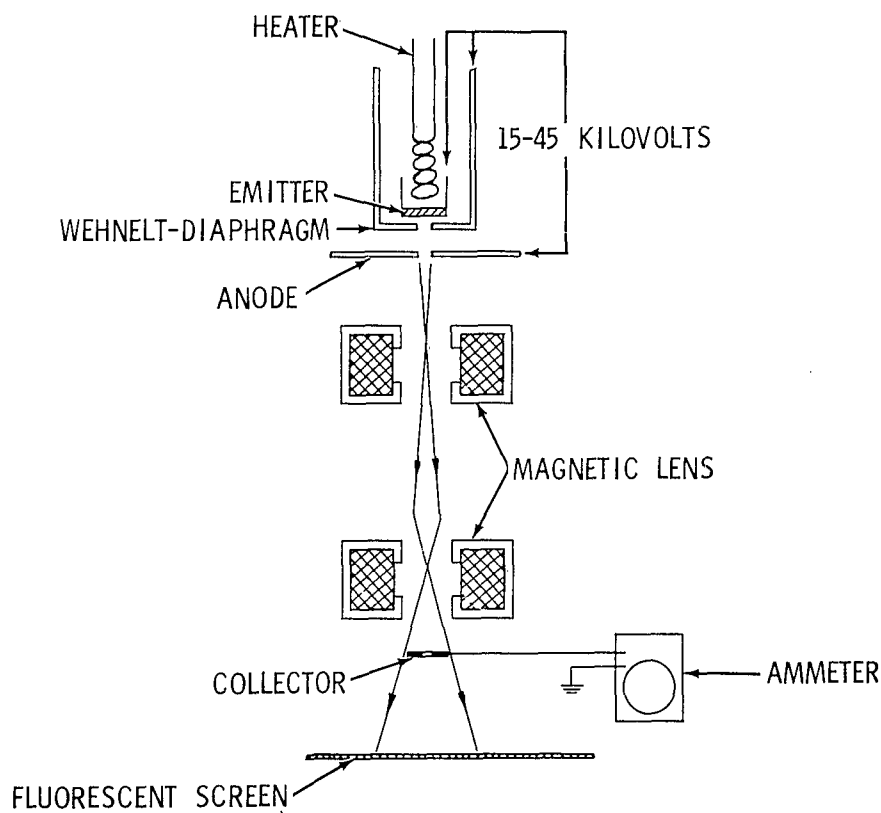


Figure 37 - Schematic of the Thermionic Emission Microscope with the collector in place.

The collector was in the form of an annular ring 1.9 cm outside diameter and 0.95 cm inside diameter. With this arrangement the emission current from a portion of the emitter could be measured while simultaneously viewing the surface of the emitter through the hole in the collector. Two parallel fiducial lines were inscribed on the surface of the emitter. The distance between these lines was

initially measured on an optical microscope. The magnification obtained in the electron emission microscope was then determined by measuring the distance between the two fiducial lines in the image produced on the fluorescent screen.

A set of experiments was conducted on a 3 mm diameter Philips cathode emitter with the collector inserted into the microscope. The emission current from the emitter was measured at various temperatures both prior and after activation of the emitter. The results of these experiments are presented in Fig. 38. Curve 'A' presents the emission current obtained from the emitter prior to activation, while curve 'B' indicated the current after activation. Activation was accomplished in this case by heating the emitter to 1205°C for three hours. Also included in Fig. 38 are photographs showing the emission patterns obtained on the microscope. These photographs are arranged at their appropriate locations on the various curves. In several of the photographs the parallel fiducial lines can be seen. For this specific emitter the fiducial lines were  $5 \times 10^{-3}$  cm apart.

Curve A, which presents the emission current from the emitter as a function of temperature prior to activation, was quite reproducible. It was interesting to note in this case that the emission current from the unactivated emitter exhibited a hysteresis loop with the temperature. In the low temperature region, the current followed the upper portion of the curve with increasing temperature and returned on the lower portion of the curve with decreasing temperature. At the high temperatures, the two portions of the curve were identical. The photographs on curve A indicate that the emitter surface was quite patchy; showing some areas where the electron emission was very high resulting from the excess barium compound on the emitter surface. The patchy areas persisted until the emitter was fully activated.

Curve B presents the emission current from the emitter after activation. In the low temperature region, the emission current from the activated emitter was about five hundred times greater than the current obtained from the unactivated emitter in the same corresponding temperature region. In this region the surface of the emitter showed a very distinct crystal structure. At about 970°C (1240°K) the emission current dropped by a factor of fifty thousand, while at the same time the surface structure changed from a crystal to a monotone pattern. From this point on the emission current increased with temperature until at 1230°C (1500°K) the current was at the same level as it was prior to the structure change. It can also be noted from the photographs that the original crystal structure reappeared at the high temperature. These surface structure changes at the various temperatures are in good agreement with the discussion presented in the previous section.

The current density of the emitter was calculated by dividing the emission current by the "corrected area" of the emitter. The corrected area of the emitter

# EMISSION CHARACTERISTICS OF A PHILIPS "B" CATHODE

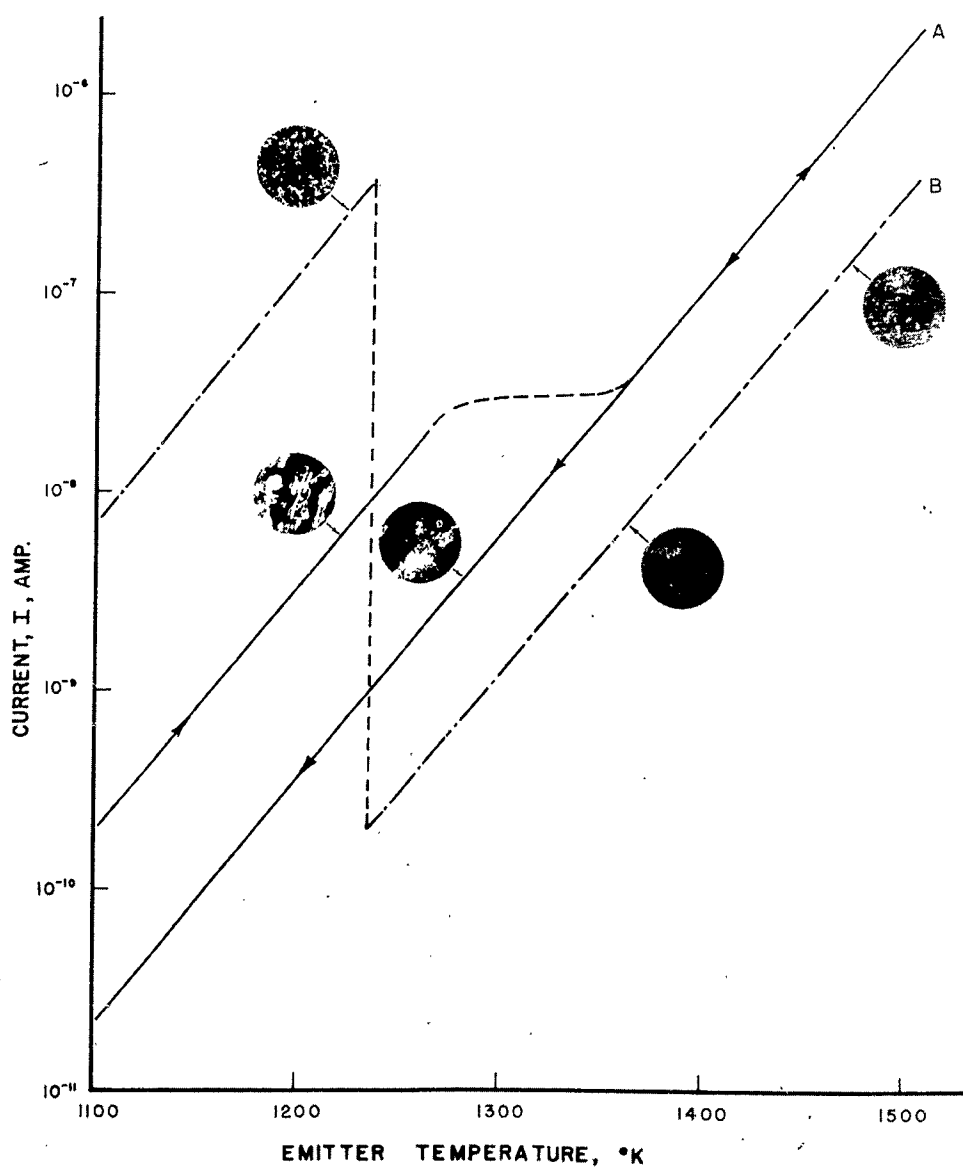


Figure 38 - Emission current from a Philips cathode emitter.



was obtained by dividing the area of the collector image that was formed on the fluorescent screen by the square of the magnification factor that was produced in the microscope. This essentially projects the collector area back to the surface of the emitter. For the data presented in Fig. 38 the corrected emitter area was calculated to be  $5.2 \times 10^{-4} \text{ cm}^2$ . The current density and effective work function based on the data from Curve B Fig. 38 are presented in Table 14.

Table 14

Current Density and Effective Work  
Function of a Philips Cathode as Obtained from the Emission Microscope

Temperature		Current Density amps/cm <sup>2</sup>	Effective Work Function, ev.
°C	°K		
830	1100	$1.6 \times 10^{-5}$	2.8
930	1200	$3 \times 10^{-4}$	2.8
1030	1300	$2 \times 10^{-6}$	3.6
1130	1400	$4 \times 10^{-5}$	3.6
1230	1500	$8 \times 10^{-4}$	3.4

From Table 14 it can be seen that the effective work functions, as calculated from the currents measured on the emission microscope, are higher than the published value of 2.1 ev at 1100°C.

The emission characteristics of the 75 v/o (60 m/o BaO - 40 m/o UO<sub>2</sub>) -25 v/o W emitter were also investigated on the emission microscope. A photograph of the emitting surface as seen on the emission microscope is shown in Fig. 39, while the current densities and effective work functions are presented in Table 15.

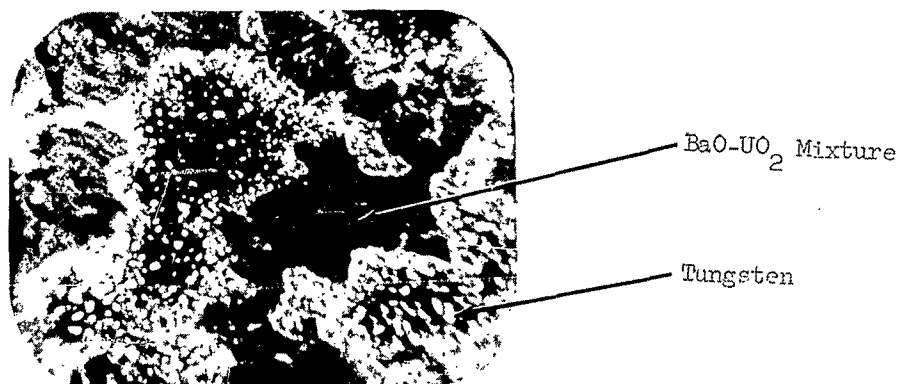


Figure 39 - Photograph of the 75 v/o (60 m/o BaO-40 m/o UO<sub>2</sub>)-25 v/o W emitter surface as recorded at 1000°C. 260 X.

Table 15

Current Density and Effective Work Function of the 75 v/o  
(60 m/o BaO-40 m/o  $\text{UO}_2$ )-25 v/o W Emitter as Obtained from the Emission Microscope

Temperature		Current Density amps/cm <sup>2</sup>	Effective Work Function, ev.
°C	°K		
830	1100	$6.9 \times 10^{-10}$	3.8
930	1200	$9.2 \times 10^{-8}$	3.7
1030	1300	$1.6 \times 10^{-5}$	3.4
1130	1400	$2.3 \times 10^{-3}$	3.1
1230	1500	$1 \times 10^{-2}$	3.1

From Fig. 39, it can be seen that the electron emission is coming predominantly from the tungsten surfaces. Activation was accomplished in this case by heating the emitter to 1100°C and holding this temperature for two hours. From Table 15 it can again be seen that the effective work functions, as calculated from the currents measured on the emission microscope, are higher than the 2.19 ev value at 1100°C as listed in Table 12. There was no evidence of a drop in emission current from this emitter at 970°C as was noted in the Philips cathode emitter.

Because of the great variation in work function as obtained from the emission microscope compared to the data presented in Table 12, various aspects of the microscope were investigated in detail. At this point there was some concern that secondary electron emission from the disc collector was producing an error in the current measurements. Under certain circumstances when a metal is subjected to bombardment by electrons, secondary electrons may be emitted. This secondary emission current may be of the same order of magnitude as the primary emission current, thus resulting in a very small current flow through the measuring circuit.

In order to investigate the degree of secondary electron emission, a Faraday cup was inserted into the microscope in place of the disc collector during the testing of the Philips cathode emitter. However, the use of the Faraday cup did not result in any increase in the measured current; indicating that secondary electron emission was negligible.

The change in emission current, as a function of the accelerating voltage used in the microscope, was also investigated. It was noted that by increasing the accelerating voltage from 15 kv to 40 kv that the emission current would increase by a factor of three. Preliminary evaluation of the emission currents obtained from the emission microscope indicated that the data cannot be intelligibly interpreted using the Schottky and Richardson correlations.

The various aspects of the emission current as measured on the thermionic emission microscope were discussed with Dr. R. D. Heidenreich of Bell Telephone Laboratories.<sup>(21)</sup> He indicated that in his work with the emission microscope he noted the same general trends, namely low current densities and high calculated work functions. After reviewing the mechanics of the emission microscope, it was postulated that the low current densities resulted from the type of electrode geometry used in the microscope. In ordinary work function measurements a simple diode is used which involves only an emitter and collector. In the emission microscope, on the other hand, a Wehnelt-diaphragm is located between the emitter and first anode. Thus the voltage profiles as seen by the emitter are greatly different in the two cases.

The voltage profile in the emission microscope is so arranged that an electron cloud may exist in front of the emitter. Only electrons with high kinetic energies are able to penetrate the electron cloud and get focused onto the fluorescent screen. These high energy electrons are still characteristic of the emitter surface thus the image produced on the fluorescent screen is representative of the emitting surface. However, the actual transmitted emission current may be greatly reduced by the electron cloud.

The density of the electron cloud may be affected by the type and pressure of gas in the microscope as well as by the materials in the emitter. For example, barium evaporation from the emitter may greatly affect the density of the electron cloud at various emitter temperatures.

Because of the complex processes that may be taking place in the emission microscope, no feasible method for evaluating the work function and emission constant of an emitter can be seen at the present time. However, the microscope can be used very profitably in evaluating the surface characteristics of various emitters.

## V. REFERENCES

1. General Motors Research Laboratories "Investigations on the Direct Conversion of Nuclear Fission Energy to Electrical Energy in a Plasma Diode", Contract No. Nonr-3109(00), October 1962, Section E.
2. Lang, S.M., Knudsen, F. P., Filmore, C.L., and Roth, R.S., "High-Temperature Reactions of Uranium Dioxide with Various Metal Oxides", NBS-568, Feb. 20, 1956.
3. Furman, S. C. "A Study of the Interaction of Barium Metal and Barium Oxide with Uranium Dioxide", KAPL-1664, Jan. 1957.
4. Trzebiatowski, W., and Jablonski, A., "Some Phase Relations of the  $\text{BaO-UO}_2\text{-O}_2$  System", Nukleonika, Vol. 5, No. 10, 1962, pp 588-595.
5. Smithells, C. J., Metals Reference Book - Vol. II, Butterworth, 1962, pp 635.
6. Chubb, W. and Rough, F. A., "An Evaluation of Data on Nuclear Carbides", Battelle Memorial Institute, BMI-1441, 1960 pp.58.
7. "JANAF Thermochemical Data", The Dow Chemical Company, Thermal Laboratory, Midland, Michigan.
8. Honig, R. E., "Vapor-Pressure Data for the Solid and Liquid Elements", RCA Review, 1962, pp 573.
9. Rittner, E. S., "A Theoretical Study of the Chemistry of the Oxide Cathode", Philips Res. Rep. 8, 1953, pp 194.
10. Hughes, R. C. and Coppola, P. P., "The Pressed Cathode", Philips Technical Review, Vol. 19, No. 6, 1957-1958 pp 177-190.
11. Brodie, I., and Jenkins, R. O., "The Evaporation of Barium from 'L' Cathodes", Journal of Electronics, July 1956, pp 45.
12. Seal Vac high vacuum fittings, Ultek Corporation, Palo Alto, California.
13. Liquid Nitrogen Level Controller, Bendix Corporation (Cincinnati), No. MPL-122.
14. Ceramic Feed Through, U. S. Stoneware Company, Smithville, Ohio, Alite No. C-250 (copper brazed).
15. Haas, G., and Harris, ., "High Accuracy X-Y Pulse Measuring System", Review of Scientific Instruments, Vol. 30, No. 8, August 1959, pp 623-625.
16. Osborne Transformer Company, 948 East Lafayette, Detroit, Michigan.
17. Rittner, Rutledge and Ahlert, "On the Mechanism of Operation of the Barium Aluminate Impregnated Cathode", Journal of Applied Physics, Vol. 28, No. 12, Dec. 1957, pp 1468.
18. Hoel, P. G., "Introduction to Mathematical Statistics", John Wiley and Sons, 1947, pp 80.
19. Hill, R. F., Rouze, S. R., "Emission Characteristics of a Philips Impregnated Cathode", Journal of Applied Physics, Vol. 33, No. 4, April 1962, pp 1607.
20. Levi, R., Improved "Impregnated Cathode", Journal of Applied Physics, Vol. 26, No. 81, May 1955, pp 639.
21. Personal communication with Dr. R. D. Heidenreich, Bell Telephone Laboratories, Murray Hill, New Jersey, March 14, 1963.

## VI. Acknowledgments

The authors wish to acknowledge the work of the Battelle Memorial Institute staff members who contributed to the evaluation of the various materials prepared in this program. Messrs. Donald Keller, Donald Kizer and Daniel Stoltz were particularly instrumental in the fabrication and evaluation of the emitter materials.

Thanks also go to the following members of the General Motors Research Laboratories for their contributions to this research program.

Messrs. Stanley Rouze and Frederic Young for their aid in conducting the various thermionic emission microscope experiments.

Dr. Frank Jamerson for his technical and administrative assistance.

Mr. Robert Aikin for his efforts in preparing and testing the various emission specimens.

Mr. Richard Dusman for his efforts in the design and fabrication of the various experimental systems.

Mr. Leonard Hockley for his work in setting up the IBM-7090 code.

Mr. John Kuhlmann for his work in preparing the drawings.

Mrs. Elizabeth LeVinge for her work as a typist and for her stenographic assistance.

## VII.

DISTRIBUTIONNo. Copies

Office of Naval Research Power Branch (Code 429) Department of the Navy Washington 25, D. C.	4
ONR Branch Office 86 East Randolph Street John Cerar Building - 10th Floor Chicago 1, Illinois Attn: Mr. M. A. Chaszeyka	1
U. S. Naval Research Laboratory Technical Information Division Washington 25, D. C.	6
Commanding Officer Office of Naval Research Branch Office Box 39 Navy No. 100 Fleet Post Office New York, New York	2
Office of Technical Services Department of Commerce Washington 25, D. C.	1
Armed Services Technical Information Agency Arlington Hall Station Arlington 12, Virginia	10
National Aeronautics and Space Administration 1520 H Street, N.W. Washington 25, D. C. Attn: James J. Lynch	1
National Aeronautics and Space Administration Lewis Research Center 2100 Brookpark Road Cleveland 35, Ohio Attn: Roland Breitwieser	1
Bernard Lubarsky	1
H. Schwartz	1
R. P. Migra	1
Wm. LeGray	1
Chief of Naval Operations (OP-07G) Department of the Navy Washington 25, D. C.	1
Commandant, U. S. Marine Corps Code CSY-3 Headquarters, Marine Corps Washington 25, D. C.	1

	<u>No. Copies</u>
Chief, Bureau of Ships	
Department of the Navy	
Washington 25, D. C.	
Attn: Code 342B	2
Code 1500 Mr. Wm. Hewitt	1
Code 456B, Mr. V. Gardner	1
Code 210L	1
 U. S. Atomic Energy Commission	
Division of Reactor Development	
Washington 25, D. C.	
Attn: Isotopic Power Branch	1
Direct Conversion Branch	1
Army Reactor and Water Systems Branch	1
SNAP Reactor Branch	1
 U. S. Atomic Energy Commission	
San Francisco Operation Office	
2111 Bancroft Way	
Berkeley 4, California	
Attn: Reactor Division	1
 Aeronautical Systems Division	
ASRMFP-2	
Wright Patterson Air Force Base	
Ohio	1
 Air Force Cambridge Research Center	
(CRZAP)	
L. G. Hanscom Field	
Bedford Massachusetts	1
 Power Information Center	
University of Pennsylvania	
Moore School Building	
200 South 33rd Street	
Philadelphia 4, Pennsylvania	1
 Director of Special Projects (SP-001)	
Department of the Navy	
Washington 25, D. C.	1
 Los Alamos Scientific Laboratory	
P. O. Box 1663	
Los Alamos, New Mexico	
Attn: Dr. George M. Grover	1
 Argonne National Laboratory	
9700 South Cass Avenue	
Argonne, Illinois	
Attn: Aaron J. Ulrich	1

	<u>No. Copies</u>
Director, Advanced Research Projects Agency The Pentagon Washington 25, D. C. Attn: Dr. John Huth	1
U. S. Army Signal R and D Laboratory Fort Monmouth, New Jersey Attn: Emil Kittl	1
General Motors Research Laboratories Library RAB 3-141	1
Atomics International P. O. Box 309 Canoga Park, California Attn: Dr. R. C. Allen	1
General Atomic P. O. Box 608 San Diego 12, California Attn: Dr. W. Pidd	1
ARACON Laboratories Virginia Road Concord, Massachusetts Attn: Dr. S. Ruby	1
Ford Instrument Company 3110 Thomson Avenue Long Island City, New York Attn: T. Jarvis	1
Armour Research Foundation 10 West 35th Street Chicago 16, Illinois Attn: Dr. D. W. Levinson	1
Jet Propulsion Laboratory California Institute of Technology 4800 Oak Grove Drive Pasadena, California Attn: P. Rouklove	1
RCA Laboratories David Sarnoff Research Center Princeton, New Jersey Attn: Dr. Paul Rappaport	1
The Martin Corporation Baltimore 3, Maryland Attn: Dr. M. Talaat	1



No. Copies

Thermo Electron Engineering Corporation  
 85 First Avenue  
 Waltham 54, Massachusetts  
 Attn: Dr. George Hatsopoulos

1

Hughes Research Laboratories  
 3011 Malibu Canyon Road  
 Malibu, California  
 Attn: Dr. R. C. Knechtli

1

Thomson Ramo Wooldridge, Inc.  
 7209 Platt Avenue  
 Cleveland 4, Ohio  
 Attn: Wm. J. Leovic

1

General Electric Research Laboratory  
 Schenectady, New York  
 Attn: Dr. V. C. Wilson

1

The Marquardt Corporation  
 ASTRO Division  
 16555 Saticoy Street  
 Van Nuys, California  
 Attn: Dr. R. Laubenstein

1

Texas Instruments, Inc.  
 P. O. Box 5474  
 Dallas 22, Texas  
 Attn: Dr. R. A. Chapman

1

University of Denver  
 Colorado Seminary  
 Denver Research Institute  
 Denver 10, Colorado  
 Attn: Dr. Charles B. Magee

1

Radio Corp. of America  
 Electron Tube Division  
 Lancaster, Pennsylvania  
 Attn: F. G. Block

1

Electro Optical Systems, Inc.  
 125 N. Halsted Avenue  
 Pasadena, California  
 Attn: A. O. Jensen

1

General Electric Company  
 P. O. Box 846  
 Atomic Product Division  
 Vallecitos Laboratory  
 Pleasanton, California  
 Attn: Robert Scott

1

	<u>No. Copies</u>
General Electric Company Power Tube Division 1 River Road Schenectady 5, New York Attn: Mr. D. L. Schaefer	1
Consolidated Controls Corporation Bethel, Connecticut Attn: Mr. David Mends	1
Institute for Defense Analysis 1666 Connecticut Avenue, N. W. Washington, D. C. Attn: Mr. Robert Hamilton	1
Knolls Atomic Power Laboratory Schenectady, New York Attn: Dr. R. Ehrlick	1

Abstract Contract Nonr-3870(00)

General Motors Research Laboratories - "Development of Barium Oxide - Uranium Oxide - Tungsten and Barium Oxide - Uranium Oxide - Rhenium Emitters for use in Nuclear Heated Thermionic Converters." F.E.Gifford and R.F.Hill (78 pages) The results of experimental and theoretical investigations that were conducted on various BaO-UO<sub>2</sub> emitter materials are presented. X-ray analysis, evaporation rate studies, thermochemical calculations, electron emission studies and thermionic emission microscope examinations are discussed in detail. The results indicate that emitters containing 60 m/o BaO and 40 m/o UO<sub>2</sub> dispersed in a matrix of either tungsten or rhenium are comparable to the commercial dispenser type emitters that employ tribarium aluminate impregnated in tungsten. The use of UO<sub>2</sub> in the emitter materials produced an emitter with a self contained heat source when operated in a nuclear environment.

Abstract Contract Nonr-3870(00)

General Motors Research Laboratories - "Development of Barium Oxide - Uranium Oxide - Tungsten and Barium Oxide - Uranium Oxide - Rhenium Emitters for use in Nuclear Heated Thermionic Converters." F.E.Gifford and R.F.Hill (78 pages) The results of experimental and theoretical investigations that were conducted on various BaO-UO<sub>2</sub> emitter materials are presented. X-ray analysis, evaporation rate studies, thermochemical calculations, electron emission studies and thermionic emission microscope examinations are discussed in detail. The results indicate that emitters containing 60 m/o BaO and 40 m/o UO<sub>2</sub> dispersed in a matrix of either tungsten or rhenium are comparable to the commercial dispenser type emitters that employ tribarium aluminate impregnated in tungsten. The use of UO<sub>2</sub> in the emitter materials produced an emitter with a self contained heat source when operated in a nuclear environment.

Abstract Contract Nonr-3870(00)

General Motors Research Laboratories - "Development of Barium Oxide - Uranium Oxide - Tungsten and Barium Oxide - Uranium Oxide - Rhenium Emitters for use in Nuclear Heated Thermionic Converters." F.E.Gifford and R.F.Hill (78 pages) The results of experimental and theoretical investigations that were conducted on various BaO-UO<sub>2</sub> emitter materials are presented. X-ray analysis, evaporation rate studies, thermochemical calculations, electron emission studies and thermionic emission microscope examinations are discussed in detail. The results indicate that emitters containing 60 m/o BaO and 40 m/o UO<sub>2</sub> dispersed in a matrix of either tungsten or rhenium are comparable to the commercial dispenser type emitters that employ tribarium aluminate impregnated in tungsten. The use of UO<sub>2</sub> in the emitter materials produced an emitter with a self contained heat source when operated in a nuclear environment.

Abstract Contract Nonr-3870(00)

General Motors Research Laboratories - "Development of Barium Oxide - Uranium Oxide - Tungsten and Barium Oxide - Uranium Oxide - Rhenium Emitters for use in Nuclear Heated Thermionic Converters." F.E.Gifford and R.F.Hill (78 pages) The results of experimental and theoretical investigations that were conducted on various BaO-UO<sub>2</sub> emitter materials are presented. X-ray analysis, evaporation rate studies, thermochemical calculations, electron emission studies and thermionic emission microscope examinations are discussed in detail. The results indicate that emitters containing 60 m/o BaO and 40 m/o UO<sub>2</sub> dispersed in a matrix of either tungsten or rhenium are comparable to the commercial dispenser type emitters that employ tribarium aluminate impregnated in tungsten. The use of UO<sub>2</sub> in the emitter materials produced an emitter with a self contained heat source when operated in a nuclear environment.